Birkbeck
UNIVERSITY OF LONDON

BIROn - Birkbeck Institutional Research Online

Ionov, D. and Doucet, L. and Pogge von Strandmann, Philip A.E. and Golovin, A. and Korsakov, A. (2017) Links between deformation, chemical enrichments and Li-isotope compositions in the lithospheric mantle of the central Siberian craton. Chemical Geology 475 , pp. 105-121. ISSN 0009-2541.

Downloaded from: https://eprints.bbk.ac.uk/id/eprint/20425/

Usage Guidelines:
Please refer to usage guidelines at https://eprints.bbk.ac.uk/policies.html or alternatively contact lib-eprints@bbk.ac.uk.

*Manuscript
Click here to download Manuscript: Text_Ud-Sheared,Li-isot_Final.docx Click here to view linked References

Links between deformation, chemical enrichments and Li-isotope compositions in the lithospheric mantle of the central Siberian craton

Dmitri A. Ionov[a,b*], Luc S. Doucet[c,d], Philip A. E. Pogge von Strandmann[e,f], Alexander V. Golovin[g,h], Andrey V. Korsakov[g,h]

[a] Géosciences Montpellier, Université de Montpellier, 34095 Montpellier, France

[b] Guangzhou Institute of Geochemistry, Chinese Academy of Sciences, 510640 Guangzhou, China

[c] Laboratoire G-Time, Université Libre de Bruxelles, 1000 Brussels, Belgium

[d] The Institute of Geosciences Research, Department of Applied Geology, Curtin University, Perth 6845, Australia

[e] London Geochemistry and Isotope Centre, Institute of Earth and Planetary Sciences, University College London and Birkbeck, University of London, London, WC1E 6BT, UK

[f] Bristol Isotope Group, School of Earth Sciences, Bristol University, Bristol, BS8 1RJ, UK.

[g] Sobolev Institute of Geology and Mineralogy, Siberian Branch Russian Academy of Sciences, Novosibirsk 630090, Russian Federation

[h] Novosibirsk State University, Novosibirsk 630090, Russian Federation

∗ Corresponding author; e-mail: dmitri.ionov@gm.univ-montp2.fr, phone: +33 (0)467143349

8950 words in the main text

ABSTRACT *(420 words)*

We report the concentrations ([Li]) and isotopic compositions of Li in mineral separates and bulk rocks obtained by MC-ICPMS for 14 previously studied peridotite xenoliths from the Udachnaya kimberlite in the central Siberian craton as well as major and trace element compositions for a new suite of 13 deformed peridotites. The deformed Udachnaya peridotites are metasomatized residues of melt extraction, which as a group experienced greater enrichments than coarse garnet and spinel peridotites. We identify two sub-groups of the deformed peridotites: (a) mainly cryptically metasomatized (similar to coarse peridotites) with relatively low modal cpx (<8%) and garnet (<10%), low Ca and high Mg#, sinusoidal REE patterns in garnet, and chemically unequilibrated garnet and cpx; (b) modally metasomatized with more cpx and garnet, higher Ca, Fe and Ti, and equilibrated garnet and cpx. The chemical enrichments are not proportional to deformation degrees. The deformation in the lower lithosphere is caused by a combination of localized stress, heating and fluid ingress from the pathways of ascending proto-kimberlite melts, with metasomatic media evolving due to reactions with wall rocks. Mg-rich olivine in spinel and coarse garnet Udachnaya peridotites has 1.2–1.9 ppm Li and δ^7Li of 1.2–5.0‰, i.e. close to olivine in equilibrated fertile to depleted off-craton mantle peridotites from literature data, whereas olivine from the deformed peridotites has much higher [Li] (2.4–7.5 ppm) and a broader range of δ^7Li (1.8-11.6‰), which we attribute to pre-eruption metasomatism. [Li] in opx is higher than in coexisting olivine while $\Delta^7Li_{Ol\text{-}Opx}$ (δ^7Li_{Ol} - δ^7Li_{Opx}) ranges from -6.6 to 7.8‰, indicating disequilibrium inter-mineral [Li] and Li-isotope partitioning. We relate these Li systematics to interaction of lithospheric peridotites with fluids or melts that are either precursors of kimberlite magmatism or products of their fractionation and/or reaction with host mantle. The melts rich in Na

and carbonates infiltrated, heated and weakened wall-rock peridotites to facilitate their deformation as well as produce high [Li] and variable, but mainly high, δ^7Li in olivine. The carbonate-rich melts preferentially reacted with the opx without achieving inter-mineral equilibrium because opx is consumed by such melts, and because of small volumes and uneven distribution of the metasomatic media, as well as short time spans between the melt infiltration and the capture of the wall-rock fragments by incoming portions of ascending kimberlite magma as xenoliths. Trapped interstitial liquid solidified as cryptic components responsible for high [Li] and the lack of δ^7Li balance between olivine and opx, and bulk rocks. These melts were Mg-poor, as shown by the unaltered δ^{26}Mg values measured in the olivine.

KEYWORDS: lithospheric mantle; Siberian craton; peridotite xenolith; lithium; Li isotopes; lithophile trace elements; deformation

1. Introduction

The most distinctive textural difference between peridotite xenoliths brought up by volcanic eruptions in cratons and those from off-craton regions is that the former include deformed porphyroclastic rocks, with coarse olivine grains partially or completely replaced with smaller polygonal neoblasts (Nixon and Boyd, 1973). Such deformed or 'sheared' peridotites are the most common rock types in many kimberlite-hosted cratonic xenolith suites. They usually contain garnet, have higher equilibration temperatures (T≥1100°C) than coarse peridotites (e.g. Boyd, 1973) and considerable chemical enrichments (e.g. Boyd, 1998).

The origins of the sheared peridotites and the extent and nature of their mantle source regions continue to be debated in spite of decades of studies (e.g. Pearson et al., 2014). Because the fine-grained textures cannot be retained for a long time in the hot mantle, they must be transient phenomena in the absence of strong differential stresses (e.g. Mercier, 1979), which are not likely to be long-lasting in cratonic lithosphere. Further, common enrichments in Fe, Ti and incompatible trace elements in sheared peridotites suggest that the deformation may be linked to metasomatism (e.g. Kesson and Ringwood, 1989), but it is not clear if the deformation comes first and triggers metasomatism by facilitating the ingress of fluids/melts or, alternatively, deformation follows mechanical weakness zones initially created by fluid ingress (e.g. van der Meer et al., 2013). Another vividly debated topic is to what extent the sheared rocks are common in cratonic lithosphere. Some lines of evidence (e.g. high density relative to normal melt-depleted peridotites due to common Fe-enrichments (Jordan, 1979) or low viscosity due to high water contents (Doucet et al., 2014)) suggest that sheared peridotites may not be a major component in cratonic lithosphere in spite of their high share in many kimberlite-hosted xenolith suites.

Instead, the strong deformation may be local and short-lived, likely limited to the lithosphere-asthenosphere boundary or, possibly, margins of mantle diapirs or pathways of kimberlitic and other fluid-rich sub-lithospheric magmas in the lithosphere (Aulbach et al., 2017; James et al., 2004; Sharygin et al., 2015).

A major hindrance in studies of kimberlite-hosted xenoliths in general and sheared rocks in particular is that they are usually serpentinized; the post-eruption alteration both obscures textural features and affects chemical compositions limiting chemical and isotope studies to analyses of coarse garnet and clinopyroxene (cpx) (e.g. Howarth et al., 2014). One of very few exceptions are samples recovered from a particular, unserpentinized portion of the Udachnaya-East kimberlite in the central Siberian craton (Golovin et al., 2017; Kamenetsky et al., 2014; Kamenetsky et al., 2012), which has arguably provided the freshest cratonic xenoliths reported so far including large sheared peridotites (Agashev et al., 2013; Ionov et al., 2010). Comprehensive studies of these rocks may further improve our knowledge of compositions and processes in cratonic lithosphere.

Very promising could be a combination of detailed petrographic and chemical data with stable isotope compositions because the latter can be fractionated by melting and metasomatism (e.g. Doucet et al., 2016; Pogge von Strandmann et al., 2011; Williams and Bizimis, 2014). In particular, studies of several mantle xenolith suites, including variably metasomatized peridotites from the SE Siberian craton (Jeffcoate et al., 2007; Magna et al., 2008; Rudnick and Ionov, 2007), have shown that Li concentrations and isotope ratios can be strongly affected by diffusion and melt-rock reaction during metasomatism. It is thus possible that Li systematics could yield new insights into fluid infiltration and element transfers if these processes accompany deformation in cratonic roots sampled by kimberlite-hosted xenoliths. No Li isotope

data for such rocks, however, have been reported as yet in peer-reviewed literature.

This paper has two new datasets and two objectives. First, we report a set of petrographic and chemical data including major and trace element compositions of whole rocks (WR) and minerals for 13 new, large and fresh, deformed peridotite xenoliths from the Udachnaya-East kimberlite, which together with previously published results (Agashev et al., 2013; Doucet et al., 2013; Ionov et al., 2010) are used to shed more light on the origin of deformed peridotites and the nature of their mantle source region both in Udachnaya and in cratonic mantle in general. Second, we report Li concentrations ([Li]) and isotope ratios for 14 peridotite xenoliths from Udachnaya-East reported by Ionov et al. (2010) and for two fresh Udachnaya kimberlites reported by Kamenetsky et al. (2012), which are the first data on Li isotopes for kimberlite-hosted mantle peridotites. These samples cover a large part of the mantle lithospheric profile beneath Udachnaya and include all major rock types of cratonic peridotites in terms of textures, modal and chemical compositions (spinel harzburgites, coarse and deformed garnet harzburgites and lherzolites). Overall, the major goal of this paper is to better constrain the relations between the textures, deformation and chemical and Li isotope composition beneath Udachnaya and in cratonic roots in general. We also report Mg-isotope ratios for olivine in four xenoliths.

2. Geologic setting and samples

2.1. *Geologic setting and host kimberlite*

The late Devonian Udachnaya pipe (66°26’ N, 112°19’E) (KML file) is part of the Daldyn-Alakit kimberlite field located in the Daldyn block near the center of the Siberian craton with crustal ages mainly 1.8–2.6 Ga (Rosen et al., 1994). The

information about regional geology, the kimberlite and its xenoliths has been provided in numerous publications including Ionov et al. (2010, 2015), Kamenetsky et al. (2012, 2014) and Moyen et al. (2017), to which readers are referred for references. The pipe was an open-pit diamond mine in 1982–2014, but from 2014 the mining and crushing was performed underground and may not recover more xenoliths. Data on Udachnaya peridotite xenoliths published before 2010 were obtained on strongly altered, serpentinized xenoliths found near the surface or at shallow levels in the mine (Boyd et al., 1997; Spetsius and Serenko, 1990). Xenoliths in this study were sampled in the 420–620 m depth range near the center of the Udachnaya-East pipe in remarkably well-preserved type-I kimberlite (Golovin et al., 2017; Kamenetsky et al., 2012; Kitayama et al., 2017). Various petrophysical, petrologic and geochemical data on samples from this study as well as other fresh, representative peridotite xenoliths from Udachnaya have been published recently (Agashev et al., 2013; Bascou et al., 2011; Doucet et al., 2013; Doucet et al., 2015; Doucet et al., 2012; Doucet et al., 2014; Goncharov et al., 2012; Ionov et al., 2015; Jean et al., 2016).

2.2. *Sample selection and preparation*

The 13 new xenoliths in this study are listed in Table 1, which provides a summary of essential petrographic and chemical data; the full dataset is given in Electronic Supplement 1 (ES1). The samples are fresh, modally homogeneous and large enough to provide representative WR powders considering their grain size and fabrics (Boyd, 1989); they include major petrographic types and deformation degrees in deformed Udachnaya peridotites. The xenoliths are ellipsoidal, 10–30 cm in size. Their rinds were removed by sawing. Slabs of fresh rock from xenolith cores were

inspected to make sure they contain no kimberlite, veins or modal gradations. Some 300–600 g (Table 1) of material were crushed to <5–10 mm in a steel jaw crusher carefully cleaned to avoid cross-contamination. Splits of crushed material (50–100 g) were ground to fine powder in agate, pure mineral grains for in-situ analyses were handpicked from other splits.

Small chips of two fresh kimberlites were crushed to ≤2 mm and inspected under binocular microscope before grinding to fine powder in agate. The crushed material was fresh, but contained numerous rounded fragments of mantle and crustal rocks or their minerals, in line with thin section observations; the most abundant xenogenic material is yellow-green olivine apparently produced by disintegration of peridotites (Kamenetsky et al., 2012; Kamenetsky et al., 2008).

The 14 xenoliths analyzed for [Li] and Li isotopes are listed in Table 2. They were selected among those reported by Ionov et al. (2010) to include all major peridotite types found as xenoliths in the Udachnaya kimberlite (including 5 deformed rocks) and to cover their P-T range (≤2.5–6.8 GPa; 760–1340°C). A summary of essential petrologic and chemical data on these samples is listed in Table 2; all available chemical data are given in Electronic Supplement 2 (ES2). Pure minerals for analyses were handpicked from 0.3–1 mm size fractions of sieved crushed rocks.

The sample preparation and analytical protocols for Udachnaya peridotites reported by Ionov et al. (2010) and Doucet et al. (2013) were the same as in this study, in particular regarding minimal alteration, modal homogeneity, lack of kimberlite veins and large size of crushed WR material as well as contamination-free WR powder preparation. By contrast, the sample preparation protocols of Udachnaya xenoliths reported by Agashev et al. (2013) were not fully specified in their paper. Anomalously high Zr in many of their WR samples suggests that their WR powders

were ground in tungsten carbide. We also use for comparison data on serpentinized Udachnaya peridotites reported by Boyd et al. (1997).

3. Analytical techniques

The concentrations of major and minor elements in 13 new whole-rock samples were determined by wavelength-dispersive (WD) X-ray fluorescence (XRF) spectrometry at J. Gutenberg University, Mainz, Germany. The rock powders were first ignited for 3 h at 1000°C to turn all FeO into Fe_2O_3 and expel water and CO_2. Loss on ignition (LOI) was calculated as mass of the powder after ignition less its mass before ignition as percentage of the initial mass. Glass beads, produced by fusing 0.8 g of the ignited powders with 4.8 g of dried LiB_4O_7 (1:7 dilution) were analyzed on a Philips PW1404 instrument using ultramafic and mafic reference samples as external standards. Ultramafic reference samples JP-1, UBN and DTS were analyzed as unknown to control accuracy with results close to recommended values (Sheet 1 of ES1). A full duplicate of sample Uv-424/09 reproduced within <0.1 wt.% for LOI, SiO_2 and MgO, ≤0.03 wt.% for other major oxides and ≤0.003 wt.% for minor oxides (Sheet 1 of ES1).

Major element compositions of minerals were obtained in grain mounts by WD electron probe micro-analysis (EPMA) at the Laboratoire Magmas et Volcans (LMV, Clermont-Ferrand, France) on a CAMECA SX-100 using 15 KeV voltage, 15 nA sample current and counting times of 20–30 s for peaks and 10 s for background; standards were natural and synthetic minerals; ZAF correction was applied.

Modal compositions were calculated from major oxide data on bulk rocks and minerals by least square regressions.

Whole-rock trace element compositions were determined by solution ICPMS (inductively coupled plasma mass spectrometer) at Université de Montpellier following a modified method of Ionov et al. (1992). Finely ground rock powders (100 mg) were dissolved in HF-$HClO_4$ mixtures. Dried samples were taken up in HNO_3 and diluted in 2% HNO_3 to 1:2000 shortly before the analysis. The solutions were analyzed on an Element XR instrument together with blanks, synthetic solutions to control oxide production and reference sample JP-1. Chemical blanks are ≤0.04 ppm for Li, Sr, Ba and Pb, and ≤0.002 ppm for Rb, Zr, Y, Nb, Ta, Cs, Hf, Th, U and rare earth elements (REE) (Sheet 2 of ES1).

Garnet and cpx were analyzed for trace elements by LA-ICPMS at the LMV in polished grain mounts. The AGILENT 7500 ICPMS instrument is coupled with an Excimer 193 nm Resonics M-50E ATL laser operated at 7 Hz, ~6 mJ.cm^{-2} pulse energy and beam size of 70–100 µm. Helium was used as carrier gas. Acquisition time was 90 s for background and 60 s for signal. SRN NIST 612 was used as external standard and BCR-g for control. Data were reduced with GLITTER software.

The concentrations and isotope ratios of Li were determined at the University of Bristol's School of Earth Sciences. Samples were dissolved in concentrated HF-HNO_3-$HClO_4$, followed by concentrated HNO_3 and 6 M HCl. $HClO_4$ was primarily used to prevent the formation of insoluble Li-fluorides (Ryan and Langmuir, 1987). Mineral separates were cleaned by ultrasonication in methanol and MQ H_2O.

Lithium concentration and isotope analysis methods are detailed in Pogge von Strandmann et al. (2011). Briefly, Li concentrations were measured on an Element 2 ICPMS using a calibration line comprising standards JP-1 ([Li] = 1.66 µg/g), BHVO-2 (4.42 µg/g) and BCR-2 (8.63 µg/g), whose concentrations were determined by isotope dilution using a 95% enriched ^{6}Li spike, which had been calibrated against a

gravimetric L-SVEC solution. JB-2 was analyzed as an unknown in every run and yielded [Li] = 7.43 ± 0.38 µg/g.

Li isotope purification was performed by passing enough sample for ~10ng Li through a two-step cation exchange column using dilute HCl as an eluent (Marschall et al., 2007; Pogge von Strandmann et al., 2011; Pogge von Strandmann et al., 2012). Li isotopes were subsequently analyzed on a Thermo Neptune multi-collector (MC) ICPMS, bracketed by the standard LSVEC. Results from international rock standards are presented in Pogge von Strandmann et al. (2011, 2012) and Lai et al. (2015). The long-term reproducibility, as determined by repeated analyses of these standards over a period of 8 years, is ±0.3‰ (2sd).

Mg isotope purification was performed by passing enough sample for ~1µg Mg through a two-step cation exchange column using dilute HNO_3 as an eluent (Pogge von Strandmann et al., 2011). Mg isotope ratios were analyzed using a Neptune MC-ICP-MS, by bracketing with the DSM-3 standard. Results from international rock standards, including an inter-laboratory comparison reported previously (Lai et al., 2015; Pogge von Strandmann et al., 2015; Pogge von Strandmann et al., 2011; Pogge von Strandmann et al., 2012; Teng et al., 2015) show that the long-term reproducibility is ±0.06‰ on δ^{26}Mg.

4. Results

4.1. *Petrography and thermo-barometry*

Cratonic garnet peridotites are commonly grouped based on their microstructures as coarse or sheared. Here we use a more detailed classification, which in addition includes a range of ‘transitional’ (from coarse to sheared) microstructures with low deformation degrees. It was proposed by Ionov et al. (2010) and further developed

by Agashev et al. (2013) and Doucet et al. (2013) for fresh Udachnaya garnet peridotites where remarkable preservation of olivine and orthopyroxene (opx) shows in detail successive transformation of granular microstructures into different porphyroclastic fabrics as the ratio of olivine neoblasts to total olivine increases from near zero to 100% (Fig. 1a-d). Here, following Ionov et al. (2010), we define the deformed fabrics as 'transitional' if the rocks: (i) have ≤60% of olivine neoblasts, and (ii) initial (pre-deformation) outlines of coarse olivine grains can be traced because the neoblasts are not displaced and their size decreases towards the former rims (Fig. 1b,c).

Among the 13 new garnet peridotites in this study seven have the transitional microstructures including one (Uv110/11) with incipient deformation (<10% neoblasts at rims of fractured coarse olivine grains; Fig. 1a) similar to those reported, together with coarse garnet peridotites, by Doucet et al. (2013), and another six are sheared including one with a 'fluidal' sub-type (Uv546/10) with chains of elongated pyroxene grains and flow marks (Fig. 1d). In terms of modal compositions (Table 1), five samples are lherzolites (12–14% cpx, 9–15% garnet) and seven are cpx-bearing harzburgites (1.6–4.9% cpx, 3–5% garnet), with an apparent gap in modal cpx (from 5 to 12%) and garnet (from 6 to 8%) between the two rock types. Out of the seven harzburgites four are sheared and three transitional, out of the five lherzolites two are sheared and three transitional, i.e. there is no apparent correlation between deformation degrees and modal compositions. The 14 samples for Li analyses (Table 2) include four spinel harzburgites, five coarse garnet harzburgites and five deformed peridotites (one transitional and four sheared; three lherzolites and two harzburgites).

The P-T estimates for the new samples are given in Table 1 and shown in Fig. 2. They range from 5.3 to 7.0 GPa and 1230 to 1315°C, with average pressures of 6.1

GPa for transitional and 6.3 GPa for sheared rocks, and the same average T~1270°C. Importantly, they overlap the highest P-T values shown by coarse garnet peridotites. Such an overlap is not uncommon in cratonic mantle, e.g. both coarse and sheared peridotites coexist in the 120-160 km depth range (~4-5 GPa, ~950-1100°C) beneath Kimberley in South Africa, indicating, like in this study, large local variations in deformation degrees (Boyd and Nixon, 1978; Katayama et al., 2009).

4.2. *Major element and modal composition*

The WR concentrations of major oxides and LOI in the 13 new samples are given in Sheet 1 of the ES1, values for Al_2O_3, FeO and CaO, and Mg# [$Mg/(Mg+Fe)_{at}$] are also provided in Table 1. The WR concentrations of major oxides and LOI in the 14 samples for Li analyses (Ionov et al., 2010) are given in Sheet 1 of the ES2. Major element compositions of minerals in the new samples are given in Sheet 3 of the ES1, those for the 14 samples for Li analyses are in Sheet 3 of the ES2.

The LOI values range from 1.0 to -0.1 wt.% (average 0.3 %); these low values indicate that secondary alteration is limited, that is, nearly absent in many samples and low in others, even in samples with abundant fine-grained olivine sensitive to alteration. The negative LOI, that is, gain of mass on ignition means that oxidation of FeO to Fe_2O_3 is more significant than the loss of volatiles (usually H_2O and CO_2 from alteration products) if the latter are present.

The contents of major and minor oxides in the peridotites in this study are plotted in Fig. 3 together with published data for fresh coarse and deformed peridotites from Udachnaya (Agashev et al., 2013; Doucet et al., 2012, 2013; Ionov et al., 2010) and for worldwide cratonic suites (recalculated to 100% anhydrous). The spinel and some coarse garnet peridotites from Udachnaya were earlier interpreted as nearly pristine

(in terms of modal and major oxide compositions) residues of 35–40% melt extraction at high to moderate pressures (Doucet et al., 2012, 2013). These residues are low in Al_2O_3 (<1.8 wt.%), CaO (<1.3 wt.%), FeO (<8 wt.%) and TiO_2 and have high NiO (>0.32 wt.%) and Mg# (≥0.92). The deformed peridotites, by contrast, usually have higher Ca, Al, Fe, Ti and lower Ni and Mg# than the coarse residual peridotites.

The deformed Udachnaya rocks in this study can be subdivided in two groups, mainly based on concentrations of Ca, Fe and Ti, and Mg#, i.e. degrees of chemical enrichment relative to typical coarse peridotites (Fig. 3). The majority (7 harzburgites) are low in Ca and contain only slightly more Fe and Ti than the residual coarse peridotites. A smaller number (5 lherzolites and a harzburgite) have much higher FeO (>9.5 wt.%) and TiO_2 (>0.1 wt.%), and low NiO (<0.3 wt.%) and Mg# (<0.89), or alternatively, high CaO (>1.5 wt.%), and plot far off the fields of coarse peridotites in Fig. 3. Some of these samples are enriched either in Fe and Ti or in Ca, but the majority show enrichments of all these elements. The ranges of SiO_2 and Cr_2O_3 in coarse and deformed garnet peridotites do not appear to be very different (Fig. 3 c,e).

The deformed Udachnaya peridotites in this study and those reported by Doucet et al. (2013) and Ionov et al. (2010) show a bi-modal distribution of modal abundances of cpx and garnet. The majority of deformed peridotites have relatively low modal cpx (<8%) and garnet (<10%), i.e. about the same as coarse garnet peridotites or only slightly higher, whereas some deformed peridotites contain notably more cpx and garnet (~12–16%) (Fig. 4 a,c). The modal distinctions between the low- and high-cpx (or low- and high-garnet) deformed peridotites are more gradual if one takes into account data for xenoliths from Udachnaya in Agashev et al. (2013) and Boyd et al. (1997) or from other cratons (Fig. 5 b,d), possibly because the modal estimates in the

latter are less precise due to small and/or heterogeneous WR samples or alteration. Yet, it is evident that the deformed Udachnaya peridotites, by contrast to coarse peridotites, include a subset of samples significantly enriched in modal cpx and garnet, as well as in Fe, Ti, Ca.

Whole-rock Mg# ($Mg\#_{WR}$) shows perfect linear correlations (correlation coefficient $r^2 = 0.99$) with Mg# of olivine ($Mg\#_{Ol}$) and opx ($Mg\#_{Opx}$) (Fig. 5a) while Cr# in WR ($Cr\#_{WR}$) shows a perfect linear correlation with Cr# of garnet ($Cr\#_{Gar}$), except for rare coarse peridotites containing accessory Cr-spinel (Fig. 5b). The $Cr\#_{WR}$ in deformed Udachnaya peridotites is identical to $Cr\#_{Gar}$; garnet appears to control the Cr-Al budgets in the rocks such that $Cr\#_{Gar}$ can be used as a proxy for $Cr\#_{WR}$. Overall, these correlations demonstrate, on the one hand, chemical equilibration of olivine, opx and garnet, and, on the other hand, the consistency and high quality of XRF (WR) and EPMA (mineral) data. No significant differences have been found between the compositions of coarse and neoblast olivine (see also Agashev et al. (2013)).

No spinel has been found in the deformed Udachnaya xenoliths, but it occurs in coarse, low-T garnet peridotites (Doucet et al., 2013) that are off the $Cr\#_{WR}$ vs. $Cr\#_{Gar}$ trend in Fig. 5b. This is consistent with thermodynamic modeling of phase relations in refractory garnet peridotites by Ziberna et al. (2013) who showed that Cr-spinel may be stable at much higher pressures (up to 5–6 GPa) at low T <1000°C, common for coarse peridotites, than at high T >1200°C (below 3–4 GPa) estimated for deformed xenoliths in this and earlier studies.

The concentrations of Ca and Al show linear correlations with modal cpx and garnet that are major mineral hosts of these elements (Fig. 6). The plot of modal garnet vs. Al_2O_3 (Fig. 6b) defines a particularly regular near-linear correlation for samples in this study, and those of Doucet et al. (2013) and Ionov et al. (2010), but

shows more scatter for samples reported by Agashev et al. (2013). The latter may be due to differences in sampling protocols, e.g. insufficient mass of WR samples, as discussed above and in *section 2.2*.

4.3. *Trace element composition*

The WR concentrations of trace elements in the 13 new samples are given in Sheet 2 of the ES1; those for the 14 samples for Li analyses after Ionov et al. (2010) are in Sheet 2 of the ES2. Trace element compositions of minerals in the 13 new samples are given in Sheet 4 of the ES1; those for the 14 samples for Li analyses are in Sheet 4 of the ES2.

Moderately incompatible trace elements in the deformed xenoliths show negative linear correlations with Al_2O_3 (r^2 >0.9 for Sc, V, Y and heavy and medium REE (Lu to Gd), and 0.80–0.87 for less compatible Zr and Hf) indicating that their concentrations are defined by melt extraction degrees. By contrast, highly incompatible elements (light REE, Rb, Sr, Nb, Ta, Pb, Th, U) show no valid correlations with Al_2O_3 and appear to be controlled by variable contributions from metasomatism. The concentrations of these elements are much higher in host kimberlites than in the xenoliths, but several elemental ratios (Nb/Ta, Rb/Cs, Ba/Nb, Ba/Rb) are distinct suggesting that mantle metasomatism rather than hypothetical contamination by kimberlite magma is the reason for enrichments of these elements in the peridotites.

The REE patterns for the new samples in this study are shown in Fig. 7 separately for eight samples with low (<6%) and five with higher (>6.5%) modal garnet. The WR samples with greater modal garnet have higher heavy and medium REE (HREE-MREE), but both groups show similar enrichments in light REE (Fig. 7 a,b). The garnets in the low-garnet xenoliths show sinusoidal or humped REE patterns with the

maximum at Eu-Sm while garnets in the high-garnet group show a gradual decrease in PM-normalized REE from Lu-Yb to La (Fig. 7c,d). The cpx in both groups (Fig. 7 e-f) have similar patterns, but those for the low-garnet rocks have lower HREE-MREE. Furthermore, the cpx/garnet ratios for the REE (Fig. 7 i-j) decrease gradually from La to Lu in the high-garnet group, in line with cpx/gar partitioning in experiments (Ghiorso et al., 2002; Smith and Asimow, 2005) and equilibrated natural samples (e.g. Ionov, 2004). By contrast, the cpx/garnet ratios in many low-garnet samples are irregular likely indicating the lack of REE equilibration between cpx and garnet. Finally, the WR REE estimates calculated from their concentrations in the cpx and garnet, and modal abundances of these minerals (Fig. 5 g-h) are similar to HREE-MREE measured in the high-garnet samples, but are more variable and commonly lower than those measured in the low-garnet samples.

The differences in REE patterns of garnets in the two groups can be illustrated with two element ratios. The Lu/Sm ratio is high in garnets from the garnet-rich rocks (with gradual decrease from HREE to MREE), but low in the garnets with 'humped' REE patterns from low-garnet rocks. The Sm/Er, by contrast, is higher in the latter than in the former. As a result, co-variation plots of Lu/Sm vs. Sm/Er in garnets or the plots of these ratios vs. modal garnet (Fig. 8) can distinguish garnets from the low- and high-garnet deformed peridotites from this and earlier work.

4.4. *Li concentrations and isotope compositions*

Lithium concentrations ([Li]) and δ^7Li determined by MC-ICPMS in pure separates of olivine and opx from 14 xenoliths, and in WR of three spinel harzburgite xenoliths and two kimberlites are given in Table 3. The variation ranges and average values ($\bar{x}$) of [Li] in olivine are similar in spinel harzburgites (1.2–1.9 ppm, $\bar{x}$ =1.5 ppm) and

coarse garnet peridotites (1.4–1.9 ppm, $\bar{x}$ =1.7 ppm), but are much greater in deformed garnet peridotites (2.4–7.5 ppm, $\bar{x}$ =4.3 ppm); those for δ^7Li in olivine increase continuously from spinel harzburgites (1.2–2.4‰, $\bar{x}$ =1.9‰) to coarse garnet peridotites (3.0–5.0‰, $\bar{x}$ =3.7‰) to deformed garnet peridotites (1.8–11.6‰, $\bar{x}$ =6.2‰) (Fig. 9a). In the opx, [Li] and δ^7Li show even greater variation ranges (Fig. 9b) and usually higher values than in olivine (Fig. 9c-d): 2.8–13.4 ppm ($\bar{x}$ =6.2 ppm) and 5.2–7.7‰ ($\bar{x}$ =6.3‰) in spinel harzburgites, 1.5–15.5 ppm ($\bar{x}$ =9.7 ppm) and 4.3–10.3‰ ($\bar{x}$ =7.1‰) in coarse garnet peridotites, and 7.7–14.1 ppm ($\bar{x}$ =11.3 ppm) and -1.9–8.0‰ ($\bar{x}$ =3.9‰) in deformed peridotites. The [Li] and δ^7Li in olivine appear to be positively correlated, with olivine from three deformed peridotites showing the highest [Li] of 4 to 7.5 ppm and δ^7Li of 7.5 to 11.6‰ (Fig. 9a).

A striking feature is the strong Li elemental and isotope disequilibrium between the coexisting olivine and opx in nearly all the samples relative to experimental results (e.g. Caciagli et al., 2011; Ottolini et al., 2009) and data on equilibrated mantle peridotites (e.g. Ionov and Seitz, 2008; Jeffcoate et al., 2007; Seitz et al., 2004). This is particularly obvious for the spinel and coarse garnet xenoliths that have a fairly narrow [Li] range (1.2–1.9 ppm) in olivine, but a much greater range (1.5–15.5 ppm) in opx (Fig. 9a). Correspondingly, the opx/olivine ratios range from 0.9 to 9 for [Li] and from 0.2 to 6.6 for δ^7Li.

Another remarkable aspect of the mineral data is the discrepancy between the [Li] from solution ICPMS analyses of mineral separates and in situ LA-ICPMS data. The LA-ICPMS [Li] available for opx cores in 11 xenoliths (Sheet 4 of ES2) range from 0.7 to 1.6 ppm ($\bar{x}$ =1.0 ppm) and show no significant differences for opx from different rock types, i.e. are 4–10 times lower than those from bulk-opx solution ICPMS analyses (2.8–15.5 ppm); the LA-ICPMS data for cpx range from 0.3 to 1.7 ppm

($\bar{x}$ =0.9 ppm) and are close to detection limit (0.1 ppm) for garnet. For the 14 new deformed samples in this study, the LA-ICPMS yielded 0.5–1.7 ppm ($\bar{x}$ =1.0 ppm) in cpx and 0.08–0.25 ppm ($\bar{x}$ =0.2 ppm) in garnet. To sum up, all available LA-ICPMS data for [Li] in opx, cpx and garnet (measured in central parts of the grains) in the Udachnaya peridotites are consistently low and distinct from the usually very high [Li] in bulk olivine and opx separates from solution ICPMS. These differences cannot be attributed to low quality of our LA-ICPMS data because earlier work showed they are reasonably consistent with solution ICPMS analyses (e.g. Rudnick and Ionov, 2007).

Bulk rock [Li] determined by solution ICPMS in earlier work on Udachnaya may be less precise than our solution ICPMS data, but they are good enough to constrain [Li] in samples that have not been analyzed in this study. [Li] in 29 fresh Udachnaya kimberlites (Kamenetsky et al., 2012) range from 11 to 52 ppm, their average (20 ppm) is similar to that for two kimberlites in this study (11 and 32 ppm, $\bar{x}$ = 21 ppm; Table 3). Average [Li] in WR Udachnaya peridotites reported by Ionov et al. (2010) increase from 4 ppm in spinel harzburgites to 5 ppm in coarse garnet peridotites to 9 ppm in deformed garnet peridotites (Sheet 2 of the ES2), i.e. are close to the [Li] range obtained for three spinel harzburgites in this study (4.9–6.7 ppm).

Importantly, the WR [Li] calculated from [Li] in minerals (solution ICPMS for olivine and opx, LA-ICPMS for cpx and garnet) and modal compositions are well below the measured [Li], e.g. 1.8–2.7 ppm vs. 4.9–6.7 ppm, respectively, for spinel peridotites (Table 3). The discrepancy between the measured and calculated WR [Li] are even greater if LA-ICPMS data are used for opx. It indicates that much Li in the rocks are hosted not by the central parts of coarse major minerals, but by their rims as well as interstitial or grain surface materials and/or unidentified micro-phases. A similar discrepancy is seen also in the measured vs. calculated δ^7Li WR values.

4.5. *Mg isotope compositions*

Table 3 gives δ^{26}Mg values for olivine separates from four xenoliths: two spinel harzburgites, one coarse garnet peridotite and one deformed garnet peridotite. They define a narrow range from -0.20‰ to -0.26‰, i.e. within the long-term reproducibility (±0.06‰), and show no significant differences between rock types, like for the majority of fertile or residual, Mg-rich on- and off-craton peridotites and pyroxenites (e.g. An et al., 2017; Lai et al., 2015; Pogge von Strandmann et al., 2011).

5. Discussion

5.1. *The origin of deformed peridotites by enrichments of melting residues*

As shown in *section 4.2*, the great majority of deformed Udachnaya peridotites are enriched in Fe and Ti, less commonly in Ca and Al, relative to coarse peridotites and model melting residues. We further subdivide them into Group 1 with low modal cpx and garnet and minor to moderate chemical enrichments, and Group 2 with higher cpx and garnet as well as usually higher Fe and Ti, and lower Ni and Mg# (Figs. 6 and 7). The formation mechanisms for these two groups may not be exactly the same. Both groups were formed by metasomatism of refractory residual peridotites, but Group 1 rocks were mainly affected by 'cryptic' metasomatism, i.e. chemical enrichments via re-equilibration of existing cpx and garnet (residual or exsolved from high-T opx; Doucet al al., 2013) with migrating melts or fluids whereas Group 2 also shows 'modal' metasomatism (Dawson, 1984), i.e. precipitation of new or additional cpx and garnet from Fe-Ti-Ca-rich melts (e.g. Shimizu, 1999). The modal cpx/garnet ratios are higher in the Group 2 than in Group 1 peridotites (0.8–1.7 vs. 0.3–1.2) indicating that the modal metasomatism could precipitate more cpx than garnet.

The enrichments in different chemical components may not be correlated to each other, e.g. the peridotite with the highest FeO (11.1 wt.%) is low in CaO and Al_2O_3 (0.8–0.9 wt.%), and in the middle of the TiO_2 range (0.12 vs. 0.05–0.22 wt.%), which may be due to metasomatism by different media, and/or by different processes (assimilation of trapped melt vs. reaction with percolating melt, e.g. Ionov et al. (2002)). The ratio of TiO_2 between coexisting garnet and cpx ranges broadly from 0.4 to 5.8 suggesting they may be out of chemical equilibrium in some samples. This inference appears to be consistent with trace element data. The sinusoidal REE in Group 1 garnets and highly variable cpx/garnet MREE-HREE ratios (Fig. 7) indicate incomplete equilibration of these minerals with (likely small-volume) metasomatic media, as earlier noted by Shimizu (1999) whereas the regular REE patterns in Group 2 garnets are consistent with greater equilibration with metasomatic media at higher melt/fluid-to-rock ratios.

5.2. *Links between deformation, chemical composition and lithospheric evolution*

Two lines of evidence could be used to infer the origin of the deformed peridotites in this study: (1) the distribution in the lithospheric profile and P-T relations of coarse vs. deformed rocks (*section 4.1*), (2) links of deformation with chemical compositions.

5.2.1 Deformed peridotites in the lithospheric profile

The following observations from the P-T data may be relevant (Fig. 2): 1) the P-T values for the deformed rocks overlap the highest values shown by the coarse rocks, i.e. both coarse and deformed peridotites occur near the base of the lithosphere (~5–7 GPa, i.e. 150-220 km depth); 2) both low-T (900-1050°C) and high-T (≥1150°C) peridotites are present in this depth range (but high-T and deformed xenoliths are most common); 3) the high-T peridotites can be either coarse or deformed; 4) the

proportion of deformed rocks decreases with depth, from 5 to 7 GPa (Goncharov et al., 2012). These observations enable to address the essential aspect of the origin of the high-T and deformed peridotites – whether they only occur near the pathways of ascending kimberlite melts or, alternatively, are unrelated to kimberlites and present throughout the lower cratonic lithosphere (e.g. Agashev et al., 2013; Ionov et al., 2010; Shimizu, 1999; van der Meer et al., 2013).

First (point 1 above), the presence and degrees (incipient-transitional → transitional → sheared → sheared-fluidal) of deformation are not correlated with temperature (Table 1) as earlier speculated by Ionov et al. (2010). Point 2 suggests non-equilibrium thermal regime in the lower 1/3 of the lithospheric mantle beneath Udachnaya at the time of kimberlite eruption (e.g. Goncharov et al., 2012), i.e. that the low- and high-T rocks are intercalated. Point 3 shows that high T alone cannot be the reason for the transformation of coarse to deformed peridotites suggesting that fluids may have played a role as well (e.g. Sharygin et al., 2015). Overall, these lines of evidence suggest that the high T near the base of the lithosphere beneath Udachnaya are caused by localized heating of wall rocks by ascending melts, and that the deformation is due to a combination of the heating, fluid ingress and stress – all related to the ascent of the proto-kimberlite melt.

5.2.2 The origin of linked deformation and chemical enrichments

We infer from the chemical evidence (*sections 4.2 and 4.3*) that the deformed Udachnaya peridotites are metasomatized residues of melt extraction, which as a group experienced greater enrichments than coarse periodites. One can envisage two tectonic settings for their formation: (1) large-scale upward melt migration from the lithosphere-asthenosphere boundary through the lower lithosphere (5-7 GPa; Fig. 2), e.g. driven by a 'super-plume' (Howarth et al., 2014; Jean et al., 2016; Pernet-

Fisher et al., 2015), (2) swarms of upward propagating conduits of proto-kimberlite melts rooted in small-scale sub-lithospheric source regions (Giuliani et al., 2016; Le Roex et al., 2003; Sharygin et al., 2015; Sun et al., 2014; van der Meer et al., 2013). The first model implies an upward zoning in the lower lithosphere with hotter and more metasomatized peridotites at greater depths, whereas the second model implies irregular distribution of temperature, deformation and enrichments with depth.

The data in this study suggest that the deformation in the Udachnaya xenoliths was accompanied mainly by small-scale, likely short-lived, enrichment events possibly involving a range of small-volume melts/fluids; more profound melt-rock reaction with additions of cpx and garnet and formation of Fe-Ti-rich rocks is less common. This style of chemical enrichments could arise in a system of thin veins spreading from ascending melt conduits, with fluid/melt compositions rapidly evolving due to mixing and reactions with host rocks, i.e. is consistent with model 2 above. By contrast, the xenoliths cannot be samples of successive zones in a large-scale upward melt migration system from the lithosphere-asthenosphere boundary. This inference is also consistent with a broad range of water in olivine (10-300 ppm) in the deepest Udachnaya peridotites (P> 5 GPa) (Doucet et al., 2014). Deformation and metasomatism may be linked also in off-craton mantle where deformed (or fine-grained recrystallized) peridotites were reported to be more metasomatized than coarse peridotites coexisting on a cm-m scale (Downes, 1990; Xu et al., 1998).

Finally, the chemical enrichments in the deformed peridotites do not appear to be proportional to deformation degrees, e.g. among the five rocks with the lowest CaO and Al_2O_3 (≤1 wt.%) four are strongly deformed (sheared, including one with fluidal fabrics); out of four Fe-enriched peridotites (9.8–11.1 wt.% FeO) three show little deformation (transitional) (Table 1). It appears that the deformation in the lithospheric

roots beneath Udachnaya was accompanied (but not caused) by a complex fluid infiltration history, which involved at least two stages. First, an early Fe-Ti-rich asthenospheric melt entered the lower lithosphere to produce localized modal and equilibrated chemical enrichments in wall-rocks over a period of time. Later on, carbonate-rich proto-kimberlite fluids rapidly ascended through the weakness zones created by the first stage of metasomatism to produce much less equilibrated reaction products accompanied by deformation driven by the violent character of kimberlite eruption (Drury and van Roermund, 1989; Kamenetsky and Yaxley, 2015).

5.3. *[Li] and Li isotopes in the mantle lithosphere beneath Udachnaya*

The elemental and isotope compositions of lithium in mantle xenoliths and mantle-derived magmas have been extensively studied in the last two decades (see a review in Penniston-Dorland et al. (2017)). However, to the best of our knowledge, this study provides the first data on [Li] and Li isotopes in kimberlite-hosted cratonic peridotites. A major reason for the lack of such data on xenoliths in kimberlites may be their widespread alteration. By contrast, the absence or low degrees of alteration in our samples enable to establish Li systematics both in bulk rocks and pure minerals.

5.3.1 Li mineral hosts and variation in Udachnaya peridotites

The main hosts of Li in peridotites, unlike for many other lithophile trace elements, are olivine and opx where it replaces Mg. Li is moderately incompatible during mantle melting, similar to Yb-Ho (Marschall et al., 2017; McDonough and Sun, 1995). Studies of unmetasomatized fertile peridotites suggested that primitive mantle has ~1.6 ppm Li and a δ^7Li of ~3.5‰ (e.g. Jeffcoate et al., 2007; McDonough and Sun, 1995; Seitz et al., 2004). Recent data on mid-ocean ridge basalts produced similar,

but possibly more precise values: ~1.39 ± 0.10 ppm Li and a δ^7Li of ~3.5 ± 1.0‰ (Marschall et al., 2017). Experimental results and data on natural samples define the following order of [Li] in minerals of equilibrated peridotites: ol > opx ≥ cpx >> gar (e.g. Caciagli et al., 2011; Ottolini et al., 2009; Seitz and Woodland, 2000).

Li isotopes were surveyed, in particular, as potential tracers of surficial materials (e.g. slab-derived) in mantle rocks and magma sources because they fractionate much more at low T. Detailed studies, however, found that [Li] and δ^7Li can be greatly affected by diffusion-driven kinetic fractionation (likely fluid-assisted) in the mantle (Aulbach and Rudnick, 2009; Jeffcoate et al., 2007; Lai et al., 2015; Lundstrom et al., 2005; Pogge von Strandmann et al., 2011; Rudnick and Ionov, 2007) and/or by interaction of xenoliths with host magma in case of extended transport and cooling (Ionov and Seitz, 2008).

As discussed above, the xenoliths in this study initially formed as melting residues and then were metasomatized, with enrichments increasing from spinel to coarse-garnet to deformed peridotites. Partial melting of fertile mantle should moderately decrease [Li] both in bulk residues, as for elements with similar compatibility (*section 4.3*), and in olivine. This appears to be the case for Mg-rich olivine in spinel and coarse garnet Udachnaya peridotites, which contains 1.2–1.9 ppm Li ($\bar{x}$ = 1.6 ppm), i.e. a little less than olivine in equilibrated fertile mantle peridotites (~1.6–2.4 ppm; Jeffcoate et al. (2007); Seitz et al. (2004)) and close to olivine in spinel harzburgite xenoliths from Kamchatka (Ionov and Seitz, 2008) ($\bar{x}$ = 1.45; Fig. 10a). By contrast, [Li] in olivine from the deformed Udachnaya peridotites (2.4–7.5 ppm) is much higher than for fertile or residual peridotites, which can only be attributed to post-melting enrichments.

Doucet et al. (2014) found strong water enrichments (up to 323 ppm H_2O in

olivine) in minerals from the deepest Udachnaya peridotites (180–220 km) and attributed them to metasomatism possibly linked to local shear zones. The olivine from the only deformed peridotite (U503) out of six samples in this study analyzed by Doucet et al. (2014) contains as much as 70 ppm water, compared to 8–26 ppm in olivine from one spinel harzburgite (U24) and four coarse garnet (U280, U283, U506, U1188) peridotites, which may be seen as evidence for links of deformation with the ingress of water-bearing fluids.

5.3.2 Non-equilibrium [Li] and Li isotopes in orthopyroxene

The fact that [Li] in opx is higher than in coexisting olivine (Figs. 9a and 10a), contrary to equilibrium inter-mineral distribution, not only supports the case for Li-enrichments by metasomatism, but also indicates that this process did not attain equilibrium. By the same token, the broad variations of $\Delta^7Li_{Ol\text{-}Opx}$ (δ^7Li_{Ol} - δ^7Li_{Opx}) from -6.6 to 7.8‰ (Table 3) imply disequilibrium inter-mineral Li-isotope partitioning (also by comparison with harzburgite xenoliths from Kamchatka (Ionov and Seitz, 2008) (Figs. 9a and 10a)).

The main reason for the erratic [Li] and Li isotope distribution may be a particular nature of opx interaction with metasomatic media in kimberlite-hosted xenoliths. Experimental work and observations on natural samples show that opx reacts with a broad range of silica-undersaturated mantle-derived melts including alkali basalts (Ionov et al., 2005b; Shaw et al., 1998), but particularly with kimberlites (Kamenetsky et al., 2009) and carbonatites (Kamenetsky and Yaxley, 2015; Sharygin et al., 2017) to produce olivine ± cpx. This is the reason why kimberlites from Udachnaya (Kamenetsky et al., 2009) and elsewhere (e.g. Arndt et al., 2010) contain abundant xenocryst and phenocryst olivine, but normally no opx.

The morphology and structure of opx grains in many samples in this study, above all in deformed peridotites, are consistent with the reaction of the opx with late-stage fluids. The opx grains in these rocks are commonly rounded to ellipsoidal, probably due to partial dissolution (Fig. 1 c,d), and have dark coatings on the surface and along cracks (probably reaction zones). Mineral fractions separated for analyses may have contained small amounts of such materials. These separates were only rinsed in distilled water, but not acid-leached before analyses, as is common in Li-isotope studies because excessive leaching may fractionate Li isotopes. Furthermore, it is possible that the rims of the corroded opx crystals were affected by Li diffusion from the reaction zones and interstitial melts. To sum up, the opx separates in this study are much more likely than olivine separates to contain components derived from metasomatic fluids, possibly Li-rich and affected by Li-isotope fractionation during emplacement and reaction with host mantle.

5.3.3 Interstitial components in the WR budget of [Li] and Li isotopes

The WR [Li] calculated from [Li] in olivine and opx and modal contents account for only 33–40% of [Li] measured in WR spinel harzburgites, while calculated WR δ^7Li (2.0–3.1‰, Table 3) are much lower than measured WR δ^7Li (7.4–9.1‰). The WR vs. mineral data suggest that much Li in the xenoliths resides in interstitial or grain-surface components. Such micro-granular materials, including Ca-rich olivine, mica, apatite, various carbonates and sulfides, have been documented in mineralogical and chemical studies of Udachnaya peridotites (Sharygin et al., 2012; Sharygin et al., 2007). Importantly, the textures and mineralogy of these materials imply an origin by precipitation from metasomatic media (likely related to kimberlites) during metasomatism or xenolith transport, and not via solidification of injected kimberlite

magma.

Important additional factors in the erratic inter-mineral [Li] and δ^7Li systematics could be that the Li enrichments: (a) were short-lived (shortly before or during eruption), and (b) involved small and unevenly distributed amounts of media with a range of [Li] and δ^7Li. Overall, we ascribe the erratic δ^7Li in our suite to the effects of kinetic Li isotope fractionation during percolation of evolving fluids from conduits into the peridotites, their reaction with opx, and diffusion of Li from the inter-granular space into and inside mineral grains (e.g. Lai et al., 2015; Lundstrom et al., 2005). All these processes apparently took place shortly before or during the eruption of the kimberlite magma accompanied by deformation in wall-rock mantle.

It is not likely, however, that the Li-isotope fractionation could be driven by different Li diffusivities of studies in mantle minerals at different temperatures (e.g. Aulbach and Rudnick, 2009; Ionov and Seitz, 2008). Recent experimental work (Yakob et al., 2012) has shown that partition coefficient for Li between olivine and diopside ($DLi_{ol/di}$ = 2.0 ± 0.2) is independent of temperature. Thus it appears that closed-system diffusion of Li between olivine and diopside (or possibly opx) in response to changing temperature is not an appropriate explanation for the observed range of elemental and isotopic distributions in natural xenoliths. An alternative could be diffusive addition or subtraction of Li during open-system interaction with an infiltrating melt or fluid (Lai et al., 2015; Pogge von Strandmann et al., 2011).

5.3.4 Effects of kimberlite contamination on [Li] and Li isotopes

Contamination by host kimberlite magma is possible on a small scale, but cannot be the major reason for [Li] and Li-isotope variations in our samples, e.g. WR δ^7Li in two spinel harzburgite xenoliths in this study are higher than in the kimberlites (Table

1). The [Li] in Udachnaya kimberlites ($\bar{x} = 21$ ppm) are not high enough to explain high [Li] in WR Udachnaya peridotites by infiltration and entrapment of their parental magma in the xenoliths, even considering that fragments of disaggregated wall-rock materials may make up about half their volume (*section 2.2*) such that [Li] (but also other incompatible trace elements) in the magmas could be twice as high as in the kimberlites. The latter are much more enriched in highly incompatible elements than in Li, such that even minor (~1-2%) contamination by kimberlite magma would be apparent in WR patterns and element ratios (Nb/Ta, Rb/Cs, Ba/Nb) of the xenoliths (*section 4.3*, Fig. 7a,b). To increase [Li] from 2 to 4 ppm would require ≥5% of trapped kimberlite magma, which would also add 9 ppm La to the peridotite, i.e. 2–11 times higher than measured WR [La], and also affect element ratios (Sheet 2 of ES2). No evidence for crosscutting kimberlite veins on a mm-scale or greater was found in hand speciemns or thin sections. Finally, experiments and natural data show that injection and assimilation of kimberlite magma in peridotites forms aggregates of cpx, mica and amphibole (e.g. Odling, 1995), which are absent in our samples.

5.3.5 Metasomatic effects on [Li] and Li isotopes: A summary

To sum up, our preferred explanation for the high WR [Li] and the erratic inter-mineral [Li] and δ^7Li distribution is interaction of lithospheric peridotites with fluids that are either precursors of kimberlite melts or, most likely, products of their fractionation and/or reaction with host mantle. The uniquely fresh host kimberlite at Udachnaya-East is rich in Na and Cl; its groundmass and melt inclusions in olivine contain alkali carbonates and other Na- and Cl-bearing minerals (Golovin et al., 2017; Golovin et al., 2007; Kamenetsky et al., 2004; Kamenetsky et al., 2014). The kimberlite melt formed in the deep mantle due to reaction of the chloride-carbonate liquids with host

peridotites; when this Si-bearing melt rises to shallow levels in the lithosphere, it crystallizes olivine and may evolve progressively toward late-stage liquids, which are potent metasomatic agents (Kamenetsky et al., 2008).

We suggest that on its way to the surface the kimberlite melt followed lithospheric shear zones and partly crystallized to yield late-stage alkali-rich melts. These highly mobile media infiltrated, heated and weakened wall-rock peridotites to facilitate their deformation as well as produce high [Li] and variable, but mainly high, δ^7Li in olivine. The metasomatism failed to yield olivine-opx inter-mineral equilibrium, because it partly consumed opx, but also because of small volumes and uneven distribution of the liquid, as well as short time spans between the melt infiltration and capture of the wall-rock fragments by the next portions of ascending kimberlite magma as deformed xenoliths. The trapped interstitial liquid solidified in the interstitial space as cryptic components responsible for high [Li] and lack of δ^7Li balance between olivine and opx on the one hand, and bulk rocks on the other hand.

Another episode of Li fractionation may have taken place following the capture of the peridotite fragments by the kimberlite magma. The ascent of the magma at the Udachnaya-East pipe was fairly rapid, probably between two hours and two days (Doucet et al., 2014), but the subsequent cooling of the intrusive kimberlite facies in the crust took much longer. The xenoliths in this study were collected 400-600 m below the surface, and the erosion may have removed a much thicker crustal section after the eruption ~360 My ago. It is reasonable to presume that the xenoliths stayed at sub-solidus temperatures long enough for alkali-rich fluids, expelled from kimberlite magma as it crystallized, to infiltrate the xenoliths, diffuse into rims of olivine and opx and further enrich the inter-granular material in Li, but not to attain equilibrium.

Modeling the isotopic fractionation shows that ^{6}Li diffuses about 5% faster than ^{7}Li in the interstitial space in the presence of fluids (Dohmen et al., 2010). Diffusion of Li in minerals is much slower, and it is much slower in olivine than in pyroxene crystals at the same conditions. Overall, a combination of diffusion along grain boundaries, in different mineral species and in grains of different size causes transient fractionation of [Li] and Li isotopes by diffusion to yield a broad range of disequilibrium [Li] and δ^{7}Li, e.g. between olivine and opx, as in xenoliths in this study (Lai et al., 2015). By contrast, mantle xenoliths rapidly transported to the surface and ejected in the air by explosive eruptions, like spinel harzburgites from Avacha, Kamchatka (Ionov and Seitz, 2008; Pogge von Strandmann et al., 2011), cooled instantaneously and show no Li enrichments and equilibrated olivine-opx [Li] and δ^{7}Li systematics.

5.4. *Mg isotopes in Udachnaya mantle peridotites*

At the same time, the late-stage melts and fluids were apparently too Mg-poor, and the mass ratio of fluid to host rock too low, to significantly affect the Mg isotope composition of measured Mg-rich olivines because the mass of Mg in the fluid was very small relative to that of Mg in the host rocks. This is why samples with high δ^{7}Li still have mantle-like δ^{26}Mg (Bourdon et al., 2010; Handler et al., 2009; Lai et al., 2015; Pogge von Strandmann et al., 2011). Magnesium isotopes also fractionate during diffusion, both at the inter-mineral (Lai et al., 2015; Pogge von Strandmann et al., 2011), and larger scale (Pogge von Strandmann et al., 2015), but documented cases of Mg isotope variation in the mantle by melt-rock reaction involved relatively Mg-rich silicate melts and high melt/rock ratios (Xiao et al., 2013). The lack of δ^{26}Mg variation therefore suggests that little Mg was contained in the metasomatising fluids

relative to the host peridotites. Overall, the samples in this study (that include major types of Udachnaya peridotites) fall in the range of typical mantle and thus suggest that large-scale Mg-isotope variations in the major part of cratonic mantle beneath Udachnaya are not likely.

6. Conclusions

1. Modal, major and trace element compositions for a new suite of 13 fresh deformed peridotites from the Udachnaya-East kimberlite in central Siberia, together with previously reported data on other samples, show that deformed garnet peridotites are metasomatized residues of melt extraction, which as a group experienced greater enrichments than coarse garnet and spinel peridotites.

2. We identify two sub-groups of the deformed peridotites: (i) cryptically metasomatized (similar to coarse peridotites) characterized by: (a) relatively low modal cpx (<8%) and garnet (<10%), (b) low Ca and high Mg#, (c) sinusoidal REE patterns in garnet, and (d) chemically unequilibrated garnet and cpx; (ii) modally metasomatized rocks with more cpx and garnet, higher Ca, Fe and Ti and equilibrated garnet and cpx.

3. The deformation in the lower cratonic lithosphere is due to a combination of localized stress, heating and fluid ingress near the pathways of ascending proto-kimberlite melts, including potent metasomatic agents that react with wall rocks. The chemical enrichments are not proportional to deformation degrees.

4. The first Li isotope data reported here for kimberlite-hosted cratonic mantle peridotites show large differences in [Li] and δ^7Li for major rock types. Olivine in coarse peridotites has [Li] and δ^7Li close to those in olivine in equilibrated fertile to depleted off-craton mantle, whereas olivine from the deformed peridotites has much

higher [Li] and a broader range of δ^7Li. We attribute the latter to reaction with liquids expelled from kimberlite melt conduits that also facilitated deformation.

5. [Li] in opx is higher than in coexisting olivine, with a broad range of $\Delta^7Li_{Ol\text{-}Opx}$.The dis-equilibrium Li partitioning does not stem from diffusive re-distribution between minerals, but is linked to interaction with external alkali-rich melts derived from ascending kimberlite magma. Large differences between [Li] determined by LA- and solution-ICPMS suggest that much Li in these rocks resides outside the “normal” Li-hosting minerals (olivine, opx) as cryptic components between the major minerals formed from trapped metasomatic media responsible for high [Li] and lack of δ^7Li balance between olivine and opx, and bulk rocks.

6. The samples in this study (that include major types of Udachnaya peridotites) show very little variation and fall in the range of typical mantle δ^{26}Mg suggesting that large-scale Mg-isotope variations in the major part of cratonic mantle in central Siberia are not likely.

Acknowledgements

We thank the ALROSA joint stock company and the open pit mine staff for access to the site and assistance with sample collection, and V. Kamenetsky for providing two kimberlite samples. DAI acknowledges funding from the French CNRS (INSU-PNP annual grants in 2010-17 for mantle studies). LSD was supported by the Belgium F.R.S.-FNRS “mandat Chargé de Recherche” n°1.B.102.14F. AVG was supported by Russian State Assignment Project 0330-2016-0006. Li and Mg isotope analyses and PPvS were funded by NERC grant NE/C510983/1.

Appendix 1. Electronic Supplement

Supplementary data associated with this article can be found in the online version, at…

References

Agashev, A.M. et al., 2013. Metasomatism in lithospheric mantle roots: Constraints from whole-rock and mineral chemical composition of deformed peridotite xenoliths from kimberlite pipe Udachnaya. Lithos, 160–161(0): 201-215.

An, Y., Huang, J.-X., Griffin, W.L., Liu, C., Huang, F., 2017. Isotopic composition of Mg and Fe in garnet peridotites from the Kaapvaal and Siberian cratons. Geochimica et Cosmochimica Acta, 200: 167-185.

Arndt, N.T. et al., 2010. Olivine, and the origin of kimberlite. J. Petrol., 51(3): 573-602.

Aulbach, S., Massuyeau, M., Gaillard, F., 2017. Origins of cratonic mantle discontinuities: A view from petrology, geochemistry and thermodynamic models. Lithos, 268–271: 364-382.

Aulbach, S., Rudnick, R.L., 2009. Origins of non-equilibrium lithium isotopic fractionation in xenolithic peridotite minerals: Examples from Tanzania. Chemical Geology, 258(1-2): 17-27.

Bascou, J. et al., 2011. Seismic velocities, anisotropy and deformation in Siberian cratonic mantle: EBSD data on xenoliths from the Udachnaya kimberlite. Earth and Planetary Science Letters, 304(1-2): 71-84.

Bernstein, S., Hanghoj, K., Kelemen, P., Brooks, C., 2006. Ultra-depleted, shallow cratonic mantle beneath West Greenland: dunitic xenoliths from Ubekendt Ejland. Contributions to Mineralogy and Petrology, 152(3): 335-347.

Bernstein, S., Kelemen, P.B., Brooks, C.K., 1998. Depleted spinel harzburgite xenoliths in Tertiary dykes from East Greenland: restites from high degree melting. Earth and Planetary Science Letters, 154(1-4): 219-233.

Bourdon, B., Tipper, E.T., Fitoussi, C., Stracke, A., 2010. Chondritic Mg isotope composition of the Earth. Geochimica et Cosmochimica Acta, 74(17): 5069-5083.

Boyd, F.R., 1973. A pyroxene geotherm. Geochimica et Cosmochimica Acta, 37(12): 2533-2546.

Boyd, F.R., 1989. Compositional distinction between oceanic and cratonic lithosphere. Earth and Planetary Science Letters, 96: 15-26.

Boyd, F.R., 1998. The origin of cratonic peridotites: a major element approach. International

Geology Review, 40(9): 755-764.

Boyd, F.R., Nixon, P.H., 1978. Ultramafic nodules from the Kimberley pipes, South Africa. Geochimica et Cosmochimica Acta, 42(9): 1367-1382.

Boyd, F.R. et al., 1997. Composition of the Siberian cratonic mantle: evidence from Udachnaya peridotite xenoliths. Contributions to Mineralogy and Petrology, 128: 228-246.

Caciagli, N., Brenan, J.M., McDonough, W.F., Phinney, D., 2011. Mineral-fluid partitioning of lithium and implications for slab-mantle interaction. Chemical Geology, 280(3-4): 384-398.

Dawson, J.B., 1984. Contrasting types of upper-mantle metasomatism? In: Kornprobst, J. (Ed.), Kimberlites II. The Mantle and Crust-Mantle Relationships. Elsevier, Amsterdam, pp. 289-294.

Dohmen, R., Kasemann, S.A., Coogan, L., Chakraborty, S., 2010. Diffusion of Li in olivine. Part I: Experimental observations and a multi species diffusion model. Geochimica et Cosmochimica Acta, 74(1): 274-292.

Doucet, L., Ionov, D., Golovin, A., 2013. The origin of coarse garnet peridotites in cratonic lithosphere: new data on xenoliths from the Udachnaya kimberlite, central Siberia. Contributions to Mineralogy and Petrology, 165(6): 1225-1242.

Doucet, L.S., Ionov, D.A., Golovin, A.V., 2015. Paleoproterozoic formation age for the Siberian cratonic mantle: Hf and Nd isotope data on refractory peridotite xenoliths from the Udachnaya kimberlite. Chemical Geology, 391(0): 42-55.

Doucet, L.S., Ionov, D.A., Golovin, A.V., Pokhilenko, N.P., 2012. Depth, degrees and tectonic settings of mantle melting during craton formation: inferences from major and trace element compositions of spinel harzburgite xenoliths from the Udachnaya kimberlite, central Siberia. Earth and Planetary Science Letters, 359–360(0): 206-218.

Doucet, L.S., Mattielli, N., Ionov, D.A., Debouge, W., Golovin, A.V., 2016. Zn isotopic heterogeneity in the mantle: A melting control? Earth and Planetary Science Letters, 451: 232–240.

Doucet, L.S. et al., 2014. High water contents in the Siberian cratonic mantle linked to metasomatism: An FTIR study of Udachnaya peridotite xenoliths. Geochimica et Cosmochimica Acta, 137(0): 159-187.

Downes, H., 1990. Shear zones in the upper mantle -- Relarion between geochemical enrichment and deformation in mantle peridotites. Geology, 18: 374-377.

Drury, M.R., van Roermund, H.L.M., 1989. Fluid assisted recrystallization in upper mantle peridotite xenoliths from kimberlites. J. Petrol., 30(pt. 1): 133-152.

Ghiorso, M.S., Hirschmann, M.M., Reiners, P.W., Kress, V.C., 2002. The pMELTS: A revision of MELTS for improved calculation of phase relations and major element

partitioning related to partial melting of the mantle to 3 GPa. Geochemistry, Geophysics, Geosystems, 3(5): 1030.

Giuliani, A., Phillips, D., Kamenetsky, V.S., Goemann, K., 2016. Constraints on kimberlite ascent mechanisms revealed by phlogopite compositions in kimberlites and mantle xenoliths. Lithos, 240–243: 189-201.

Golovin, A.V., Sharygin, I.S., Korsakov, A.V., 2017. Origin of alkaline carbonates in kimberlites of the Siberian craton: Evidence from melt inclusions in mantle olivine of the Udachnaya-East pipe. Chemical Geology, (in press), doi: 10.1016/j.chemgeo.2016.10.036.

Golovin, A.V., Sharygin, V.V., Pokhilenko, N.P., 2007. Melt inclusions in olivine phenocrysts in unaltered kimberlites from the Udachnaya-East pipe, Yakutia: some aspects of kimberlite magma evolution during late crystallization stages. Petrology 15: 168–183.

Goncharov, A.G., Ionov, D.A., Doucet, L.S., Pokhilenko, L.N., 2012. Thermal state, oxygen fugacity and C-O-H fluid speciation in cratonic lithospheric mantle: new data on peridotite xenoliths from the Udachnaya kimberlite, Siberia. Earth and Planetary Science Letters, 357-358: 99-110.

Handler, M.R., Baker, J.A., Schiller, M., Bennett, V.C., Yaxley, G.M., 2009. Magnesium stable isotope composition of Earth's upper mantle. Earth and Planetary Science Letters, 282(1-4): 306-313.

Herzberg, C., 2004. Geodynamic information in peridotite petrology. Journal of Petrology, 45(12): 2507-2530.

Holland, T.J.B., Powell, R., 1998. An internally-consistent thermodynamic dataset for phases of petrological interest. Journal of Metamorphic Geology, 16: 309-344.

Howarth, G.H. et al., 2014. Superplume metasomatism: Evidence from Siberian mantle xenoliths. Lithos, 184–187(0): 209-224.

Ionov, D.A., 2004. Chemical variations in peridotite xenoliths from Vitim, Siberia: inferences for REE and Hf behaviour in the garnet facies upper mantle. Journal of Petrology, 45(2): 343-367.

Ionov, D.A., 2007. Compositional variations and heterogeneity in fertile lithospheric mantle: peridotite xenoliths in basalts from Tariat, Mongolia. Contrib. Mineral. Petrol., 154(4): 455-477.

Ionov, D.A., Ashchepkov, I., Jagoutz, E., 2005a. The provenance of fertile off-craton lithospheric mantle: Sr-Nd isotope and chemical composition of garnet and spinel peridotite xenoliths from Vitim, Siberia. Chemical Geology, 217(1-2): 41-75.

Ionov, D.A., Bodinier, J.-L., Mukasa, S.B., Zanetti, A., 2002. Mechanisms and sources of mantle metasomatism: major and trace element compositions of peridotite xenoliths from Spitsbergen in the context of numerical modeling. Journal of Petrology, 43(12):

2219-2259.

Ionov, D.A., Chanefo, I., Bodinier, J.-L., 2005b. Origin of Fe-rich lherzolites and wehrlites from Tok, SE Siberia by reactive melt percolation in refractory mantle peridotites. Contributions to Mineralogy and Petrology, 150(3): 335-353.

Ionov, D.A., Doucet, L.S., Ashchepkov, I.V., 2010. Composition of the lithospheric mantle in the Siberian craton: new constraints from fresh peridotites in the Udachnaya-East kimberlite. Journal of Petrology, 51(11): 2177-2210.

Ionov, D.A., Doucet, L.S., Carlson, R.W., Golovin, A.V., Korsakov, A.V., 2015. Post-Archean formation of the lithospheric mantle in the central Siberian craton: Re–Os and PGE study of peridotite xenoliths from the Udachnaya kimberlite. Geochimica et Cosmochimica Acta, 165: 466-483.

Ionov, D.A., Hofmann, A.W., 2007. Depth of formation of sub-continental off-craton peridotites. Earth and Planetary Science Letters, 261(3-4): 620-634.

Ionov, D.A., Savoyant, L., Dupuy, C., 1992. Application of the ICP-MS technique to trace element analysis of peridotites and their minerals. Geostandards Newsletter, 16(2): 311-315.

Ionov, D.A., Seitz, H.-M., 2008. Lithium abundances and isotopic compositions in mantle xenoliths from subduction and intra-plate settings: mantle sources vs. eruption histories. Earth and Planetary Science Letters, 266(3-4): 316-331.

Irvine, G.J. et al., 2003. A Re-Os isotope and PGE study of kimberlite-derived peridotite xenoliths from Somerset Island and a comparison to the Slave and Kaapvaal cratons. Lithos, 71(2-4): 461-488.

James, D.E., Boyd, F.R., Schutt, D., Bell, D.R., Carlson, R.W., 2004. Xenolith constraints on seismic velocities in the upper mantle beneath southern Africa. Geochem. Geophys. Geosyst., 5(1): Q01002.

Jean, M.M. et al., 2016. Olivine inclusions in Siberian diamonds and mantle xenoliths: Contrasting water and trace-element contents. Lithos, 265: 31-41.

Jeffcoate, A.B. et al., 2007. Li isotope fractionation in peridotites and mafic melts. Geochimica et Cosmochimica Acta, 71(1): 202-218.

Jordan, T.H., 1979. Mineralogies, densities and seismic velocities of garnet lherzolites and their geophysical implications. In: Boyd, F.R., Meyer, H.O.A. (Eds.), The Mantle Sample: Inclusions in Kimberlites and Other Volcanics. Am. Geophys. Union, Washington, D.C., pp. 1-14.

Kamenetsky, M.B. et al., 2004. Kimberlite melts rich in alkali chlorides and carbonates: A potent metasomatic agent in the mantle. Geology, 32(10): 845-848.

Kamenetsky, V.S. et al., 2014. Towards a new model for kimberlite petrogenesis: Evidence from unaltered kimberlites and mantle minerals. Earth-Science Reviews, 139(0): 145-

167.

Kamenetsky, V.S., Kamenetsky, M.B., Golovin, A.V., Sharygin, V.V., Maas, R., 2012. Ultrafresh salty kimberlite of the Udachnaya–East pipe (Yakutia, Russia): A petrological oddity or fortuitous discovery? Lithos, 152: 173-186.

Kamenetsky, V.S. et al., 2008. Olivine in the Udachnaya-East kimberlite (Yakutia, Russia): Types, compositions and origins. Journal of Petrology, 49(4): 823-839.

Kamenetsky, V.S. et al., 2009. Can pyroxenes be liquidus minerals in the kimberlite magma? Lithos, 112(Supplement 1): 213-222.

Kamenetsky, V.S., Yaxley, G.M., 2015. Carbonate–silicate liquid immiscibility in the mantle propels kimberlite magma ascent. Geochimica et Cosmochimica Acta, 158(0): 48-56.

Katayama, I., Suyama, Y., Ando, J.-i., Komiya, T., 2009. Mineral chemistry and P-T condition of granular and sheared peridotite xenoliths from Kimberley, South Africa: Origin of the textural variation in the cratonic mantle. Lithos, 109(3-4): 333-340.

Kesson, S.E., Ringwood, A.E., 1989. Slab-mantle interactions: 1. Sheared and refertilised garnet peridotite xenoliths — samples of Wadati-Benioff zones? Chemical Geology, 78(2): 83-96.

Kitayama, Y. et al., 2017. Co-magmatic sulfides and sulfates in the Udachnaya-East pipe (Siberia): A record of the redox state and isotopic composition of sulfur in kimberlites and their mantle sources. Chemical Geology, (in press), doi: 10.1016/j.chemgeo.2016.10.037.

Kopylova, M.G., Russell, J.K., 2000. Chemical stratification of cratonic lithosphere: constraints from the Northern Slave craton, Canada. Earth and Planetary Science Letters, 181(1-2): 71-87.

Lai, Y.-J., Pogge von Strandmann, P.A.E., Dohmen, R., Takazawa, E., Elliott, T., 2015. The influence of melt infiltration on the Li and Mg isotopic composition of the Horoman Peridotite Massif. Geochimica et Cosmochimica Acta, 164(0): 318-332.

Le Roex, A.P., Bell, D.R., Davis, P., 2003. Petrogenesis of Group I Kimberlites from Kimberley, South Africa: Evidence from Bulk-rock Geochemistry. J. Petrology, 44(12): 2261-2286.

Lee, C.-T., Rudnick, R.L., 1999. Compositionally stratified cratonic lithosphere: petrology and geochemistry of peridotite xenoliths the Labait volcano, Tanzania. In: Gurney, J.J., Gurney, J.L., Pascoe, M.D., Richardson, S.H. (Eds.), Proc. 7th Internatl. Kimberlite Conf. RedRoof Design, Cape Town, pp. 503-521.

Lundstrom, C.C., Chaussidon, M., Hsui, A.T., Kelemen, P., Zimmerman, M., 2005. Observations of Li isotopic variations in the Trinity Ophiolite: Evidence for isotopic fractionation by diffusion during mantle melting. Geochimica et Cosmochimica Acta, 69(3): 735-751.

Magna, T., Ionov, D.A., Oberli, F., Wiechert, U., 2008. Links between mantle metasomatism and lithium isotopes: Evidence from glass-bearing and cryptically metasomatized xenoliths from Mongolia. Earth and Planetary Science Letters, 276(1–2): 214-222.

Marschall, H.R., Pogge von Strandmann, P.A.E., Seitz, H.-M., Elliott, T., Niu, Y., 2007. The lithium isotopic composition of orogenic eclogites and deep subducted slabs. Earth Planet. Sci. Lett., 262(3-4): 563-580.

Marschall, H.R. et al., 2017. The boron and lithium isotopic composition of mid-ocean ridge basalts and the mantle. Geochimica et Cosmochimica Acta, 207: 102-138.

McDonough, W.F., Sun, S.-s., 1995. The composition of the Earth. Chemical Geology, 120: 223-253.

Mercier, J.-C.C., 1979. Peridotite xenoliths and the dynamics of kimberlite intrusion, The Mantle Sample: Inclusion in Kimberlites and Other Volcanics. American Geophysical Union, pp. 197-212.

Nixon, P.H., Boyd, F.R., 1973. Petrogenesis of the granular and sheared ultrabasic nodule suite in kimberlite. In: Nixon, P.H. (Ed.), Lesotho Kimberlites. Lesotho Nat. Dev. Corp., Maseru, pp. 48-56.

Odling, N.W.A., 1995. An experimental replication of upper-mantle metasomatism. Nature, 373(1): 58-60.

Ottolini, L., Laporte, D., Raffone, N., Devidal, J.-L., Le Fèvre, B., 2009. New experimental determination of Li and B partition coefficients during upper mantle partial melting. Contributions to Mineralogy and Petrology, 157(3): 313-325.

Pearson, D.G., Canil, D., Shirey, S.B., 2014. Mantle Samples Included in Volcanic Rocks: Xenoliths and Diamonds. In: Carlson, R.W. (Ed.), Treatise on Geochemistry (Second Edition). Elsevier, Oxford, pp. 169-253.

Pearson, D.G., Irvine, G.J., Ionov, D.A., Boyd, F.R., Dreibus, G.E., 2004. Re-Os isotope systematics and platinum group element fractionation during mantle melt extraction: a study of massif and xenolith peridotite suites. Chemical Geology, 208(1-4, Highly Siderophile Element Behavior in High Temperature Processes): 29-59.

Penniston-Dorland, S., Liu, X.-M., Rudnick, R.L., 2017. Lithium Isotope Geochemistry. Reviews in Mineralogy and Geochemistry, 82(1): 165.

Pernet-Fisher, J.F. et al., 2015. Plume impingement on the Siberian SCLM: Evidence from Re–Os isotope systematics. Lithos, 218–219(0): 141-154.

Pogge von Strandmann, P.A.E., Dohmen, R., Marschall, H.R., Schumacher, J.C., Elliott, T., 2015. Extreme magnesium isotope fractionation at outcrop scale records the mechanism and rate at which reaction fronts advance. Journal of Petrology, 56(1): 33-58.

Pogge von Strandmann, P.A.E. et al., 2011. Variations of Li and Mg isotope ratios in bulk

chondrites and mantle xenoliths. Geochimica et Cosmochimica Acta, 75(18): 5247-5268.

Pogge von Strandmann, P.A.E. et al., 2012. Lithium, magnesium and silicon isotope behaviour accompanying weathering in a basaltic soil and pore water profile in Iceland. Earth and Planetary Science Letters, 339–340: 11-23.

Pollack, H.N., Chapman, D.S., 1977. On the regional variation of heat flow, geotherms and lithospheric thickness. Tectonophysics, 38: 279-296.

Rosen, O.M., Condie, K.C., Natapov, L.M., Nozhkin, A.D., 1994. Archean and Early Proterozoic evolution of the Siberian craton: a preliminary assessment. In: Condie, K.C. (Ed.), Archean Crustal Evolution. Elsevier, Amsterdam, pp. 411-459.

Rudnick, R.L., Ionov, D.A., 2007. Lithium elemental and isotopic disequilibrium in minerals from peridotite xenoliths from far-east Russia: product of recent melt/fluid-rock reaction. Earth Planet. Sci. Lett., 256(1-2): 278-293.

Ryan, J.G., Langmuir, C.H., 1987. The systematics of lithium abundances in young volcanic rocks. Geochimica et Cosmochimica Acta, 51(6): 1727-1741.

Seitz, H.M., Brey, G.P., Lahaye, Y., Durali, S., Weyer, S., 2004. Lithium isotopic signatures of peridotite xenoliths and isotopic fractionation at high temperature between olivine and pyroxenes. Chemical Geology, 212(1-2): 163-177.

Seitz, H.M., Woodland, A.B., 2000. The distribution of lithium in peridotitic and pyroxenitic mantle lithologies - An indicator of magmatic and metasomatic processes. Chem. Geol., 166(1–2): 47-64.

Sharygin, I.S., Golovin, A.V., Pokhilenko, N.P., 2012. Djerfisherite in xenoliths of sheared peridotite in the Udachnaya-East pipe (Yakutia): origin and relationship with kimberlitic magmatism. Russian Geology and Geophysics, 53: 247-261.

Sharygin, I.S. et al., 2015. Melting phase relations of the Udachnaya-East Group-I kimberlite at 3.0–6.5 GPa: Experimental evidence for alkali-carbonatite composition of primary kimberlite melts and implications for mantle plumes. Gondwana Research, 28(4): 1391-1414.

Sharygin, I.S. et al., 2017. Experimental constraints on orthopyroxene dissolution in alkali-carbonate melts in the lithospheric mantle: Implications for kimberlite melt composition and magma ascent. Chemical Geology: (in press) 10.1016/j.chemgeo.2016.09.030.

Sharygin, V.V., Golovin, A.V., Pokhilenko, N.P., Kamenetsky, V.S., 2007. Djerfisherite in the Udachnaya-East pipe kimberlites (Sakha-Yakutia, Russia): paragenesis, composition and origin. European Journal of Mineralogy, 19(1): 51-63.

Shaw, C.S.J., Thibault, Y., Edgar, A.D., Lloyd, F.E., 1998. Mechanisms of orthopyroxene dissolution in silica-undersaturated melts at 1 atmosphere and implications for the

origin of silica-rich glass in mantle xenoliths. Contrib. Mineral. Petrol., 132: 354-370.

Shimizu, N., 1999. Young geochemical features in cratonic peridotites from Southern Africa and Siberia. In: Fei, Y., Bertka, C.M., Mysen, B.O. (Eds.), Mantle Petrology: Field Observations and High-Pressure Experimentation. Spec. Publ. Geochem. Soc. No. 6. Geochemical Society, Houston, pp. 47-55.

Simon, N.S.C., Carlson, R.W., Pearson, D.G., Davies, G.R., 2007. The origin and evolution of the Kaapvaal cratonic lithospheric mantle. Journal of Petrology, 48(3): 589-625.

Smith, P.M., Asimow, P.D., 2005. Adiabat_1ph: A new public front-end to the MELTS, pMELTS, and pHMELTS models. Geochemistry, Geophysics, Geosystems, 6(2): Q02004.

Spetsius, Z.V., Serenko, V.P., 1990. Composition of the continental upper mantle and lower crust beneath the Siberian Platform. Nauka, Moscow, 272 (in Russian) pp.

Sun, J. et al., 2014. Repeated kimberlite magmatism beneath Yakutia and its relationship to Siberian flood volcanism: Insights from in situ U–Pb and Sr–Nd perovskite isotope analysis. Earth and Planetary Science Letters, 404(0): 283-295.

Teng, F.-Z. et al., 2015. Interlaboratory comparison of magnesium isotopic compositions of 12 felsic to ultramafic igneous rock standards analyzed by MC-ICPMS. Geochemistry, Geophysics, Geosystems, 16(9): 3197-3209.

van der Meer, Q.H.A., Klaver, M., Waight, T.E., Davies, G.R., 2013. The provenance of sub-cratonic mantle beneath the Limpopo Mobile Belt (South Africa). Lithos, 170–171: 90-104.

Williams, H.M., Bizimis, M., 2014. Iron isotope tracing of mantle heterogeneity within the source regions of oceanic basalts. Earth and Planetary Science Letters, 404(0): 396-407.

Wittig, N. et al., 2008. Origin of cratonic lithospheric mantle roots: A geochemical study of peridotites from the North Atlantic Craton, West Greenland. Earth and Planetary Science Letters, 274(1-2): 24-33.

Xiao, Y., Teng, F.-Z., Zhang, H.-F., Yang, W., 2013. Large magnesium isotope fractionation in peridotite xenoliths from eastern North China craton: Product of melt–rock interaction. Geochimica et Cosmochimica Acta, 115: 241-261.

Xu, Y., Menzies, M.A., Vroon, P., Mercier, J.-C., Lin, C., 1998. Texture-temperature-geochemistry relationships in the upper mantle as revealed from spinel peridotite xenoliths from Wangqing, NE China. J. Petrol., 39(3): 469-493.

Yakob, J.L., Feineman, M.D., Deane Jr, J.A., Eggler, D.H., Penniston-Dorland, S.C., 2012. Lithium partitioning between olivine and diopside at upper mantle conditions: An experimental study. Earth and Planetary Science Letters, 329–330(0): 11-21.

Ziberna, L., Klemme, S., Nimis, P., 2013. Garnet and spinel in fertile and depleted mantle:

insights from thermodynamic modelling. Contributions to Mineralogy and Petrology, 166(2): 411-421.

Figure captions

Fig. 1. Photomicrographs of deformed Udachnaya garnet peridotites in this study in transmitted plane-polarized light; *scale bars are at bottom left, sample numbers are at upper left*. *Ol* olivine, *Opx* orthopyroxene, *Cpx* clinopyroxene, *Gar* garnet. Plates ***a*** to ***d*** illustrate successive transformation of initially granular rocks into a range of porphyroclastic microstructures as the ratio of olivine neoblasts to total olivine increases from near zero to 100% (Fig. 1a-z): **a** Incipient deformation with rare (<10%) subgrains and neoblasts at rims of fractured coarse olivine; **b-c** transitional deformation: <60–80% of olivine neoblasts, initial outlines of coarse olivine grains discernible because the neoblasts are not displaced and their size decreases towards the former rims; **d** sheared (all olivine as fine-grained neoblasts) with elongated grains and clusters of opx, rare rounded grains of garnet and cpx and thin streaks of dark microcrystalline material.

Fig. 2. Plots of pressure (P) vs. temperature (T) estimates for deformed Udachnaya peridotites in this study (large blue circles) using the opx-gar barometer of Nickel and Green (1985) (P_{NG85}) coupled with (**a**) the cpx-opx thermometer of Taylor (1998) (TTA_{98}), and (**b**) the Ca-in-opx thermometer of Brey and Köhler (1990) corrected as in Nimis and Grütter (2010) ($T_{Ca\text{-}in\text{-}opx}$). Also shown are coarse (small red circles) and deformed (small green circles) Udachnaya peridotites after Doucet et al. (2013), the fields of Udachnaya deformed peridotites reported by Agashev et al. (2013) and of spinel peridotites (estimated by projecting T values to the 40 mW/m^2 geotherm, Goncharov et al. (2012)), model conductive geotherms after Pollack and Chapman

(1977), graphite/diamond (G/D) stability boundary (Holland and Powell, 1998) and mantle adiabats for T_p=1250°C and 1300°C.

Fig. 3. Co-variation plots of Al_2O_3 (a robust melt extraction index) with major and minor oxides (wt.%) for whole-rock deformed garnet peridotites in this study, published data on coarse and deformed garnet peridotites, and spinel harzburgites from Udachnaya (Agashev et al., 2013; Doucet et al., 2012, 2013; Ionov et al., 2010), see (e) and (f) for symbols. Also shown are primitive mantle (PM) after McDonough and Sun (1995); fertile off-craton garnet and spinel peridotite xenoliths from central Asia (fine dashed contours; Ionov (2007); Ionov et al. (2005a); Ionov and Hofmann (2007)); Horoman massif peridotites (grey contours; Takazawa et al. 2000); peridotite xenoliths (thin crosses) from the Kaapvaal (Pearson et al., 2004; Simon et al., 2007), Tanzanian (Lee and Rudnick, 1999), North Atlantic (Bernstein et al., 2006; Bernstein et al., 1998; Wittig et al., 2008) and Slave (Irvine et al., 2003; Kopylova and Russell, 2000) cratons. Thick continuous lines are residues of polybaric fractional melting of fertile mantle at 2–0, 3–0, 5–1 and 7–2 GPa (Herzberg, 2004). Deformed Udachnaya peridotites diverge more from melt extraction trends, hence experienced more metasomatism, than coarse rocks.

Fig. 4. Histograms of modal clinopyroxene and garnet in deformed Udachnaya peridotites in this study in comparison with data for coarse garnet peridotites after Doucet et al. (2013) and Ionov et al. (2010) (a, c), and for coarse and deformed garnet peridotites from Udachnaya (Agashev et al., 2013; Boyd et al., 1997) and other cratonic localities (b, d). Two groups of deformed peridotites can be identified: one low in cpx and garnet (group 1), the other high in cpx and garnet (group 2).

Fig. 5. Co-variation plots for Mg# [$Mg/(Mg+Fe)_{at}$] in whole-rocks (WR) and in olivine (Ol) and orthopyroxene (Opx) in this study (a), and for Cr# [$Cr/(Cr+Al)_{at}$] in WR and

garnet for Udachnaya xenoliths in this study and those in Doucet et al. (2013) and Ionov et al. (2010) (b). Four coarse peridotites with high Cr# in WR in (b) contain accessory Cr-spinel. Excellent linear correlations in (a, b) demonstrate analytical quality (XRF and EPMA) and major oxide equilibration of minerals in the rocks; they also confirm that the material crushed to obtain whole-rock powders is representative of the rocks in terms of homogeneity and mass. Symbols are the same as in Fig. 2.

Fig. 6. Co-variation plots of whole-rock (WR) Al_2O_3 (wt.%) vs. modal cpx (a) and garnet (b) in peridotite xenoliths from Udachnaya and other mantle peridotites. Two groups of deformed peridotites, low- and high-cpx, in (a), and an excellent linear correlation for garnet peridotites from this study, Doucet et al. (2013) and Ionov et al. (2010) in (b) are to be noted. Symbols are the same as in Fig. 2.

Fig. 7. Primitive mantle-normalized (McDonough and Sun, 1995) rare earth element (REE) patterns for WR and minerals of deformed garnet peridotites in this study, top to bottom: whole-rocks (a-b), garnet (c-d), clinopyroxene e-f), whole-rocks calculated from mineral data (g-h), and cpx/gar ratios (i-j). The columns on the left and on the right are, respectively, for samples with <6.5% and >6.5% of modal garnet. Low-garnet peridotites have lower middle and heavy REE in WR and cpx than high-garnet peridotites, 'sinusoidal' REE patterns with a minimum for Dy-Tb and a 'hump' for Gd-Sm, and cpx apparently out of equilibrium with garnet for heavy and middle REE. By contrast, the high-garnet samples show gradual decrease in REE in garnet from Lu to La, and coherent cpx and garnet patterns.

Fig. 8. Plots of PM-normalized (McDonough and Sun, 1995) Lu/Sm_N and Sm/Er_N in garnet vs. modal garnet for Udachnaya peridotites in this study and in Doucet et al. (2013) distinguish the peridotites with low and high modal garnet (and cpx) because of differences in their REE patterns (sinusoidal vs. gradual Lu-to-La depletion). The

sinusoidal garnets in low-garnet peridotites show a combination of low Lu/Sm and high Sm/Er. By contrast, the garnets in rocks with high modal garnet have high Lu/Sm and low Sm/Er (see Fig. 7 c-d for REE patterns in garnet).

Fig. 9. Co-variation plots of Li concentration ([Li]) and δ^7Li in olivine and opx in Udachnaya xenoliths in this study. The long-term reproducibility of δ^7Li, as determined by repeated analyses of reference materials, is ±0.3‰ (2sd). Also shown are fields for olivine in normal mantle (PM) from studies of pristine, fertile mantle peridotite xenoliths (Ionov and Seitz, 2008; Jeffcoate et al., 2007; Seitz et al., 2004) and spinel harzburgites from Kamchatka hosted by andesitic scoria (instantaneous cooling on eruption) (Ionov and Seitz, 2008). To be noted are a positive [Li] vs. δ^7Li correlation for olivine (a), higher [Li] and δ^7Li in opx than in coexisting olivine in coarse peridotites (b, c), and broad, erratic variations of both [Li] and δ^7Li in deformed xenoliths, particularly by comparison to narrow variation ranges in the equilibrated Kamchatka with similar modal compositions.

Fig. 10. Co-variation plots of Li concentration (a) and δ^7Li (b) in olivine and opx vs. Mg# in olivine; also shown are olivine in spinel harzburgites from Kamchatka (Ionov and Seitz, 2008) and estimates for olivine in primitive mantle (PM) (Jeffcoate et al., 2007; McDonough and Sun, 1995; Seitz et al., 2004).

Figure
Click here to download high resolution image

Fig. 1

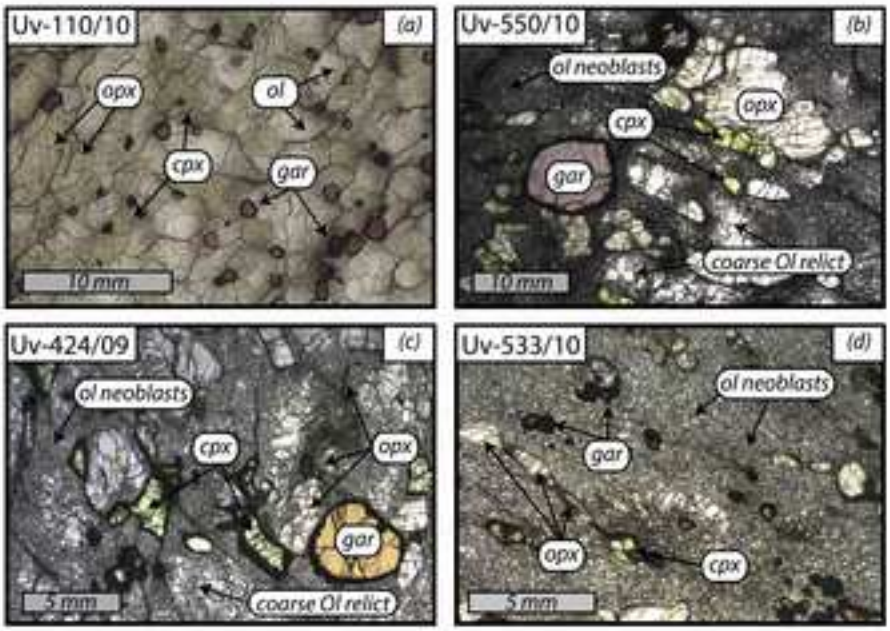

Figure

Fig. 2

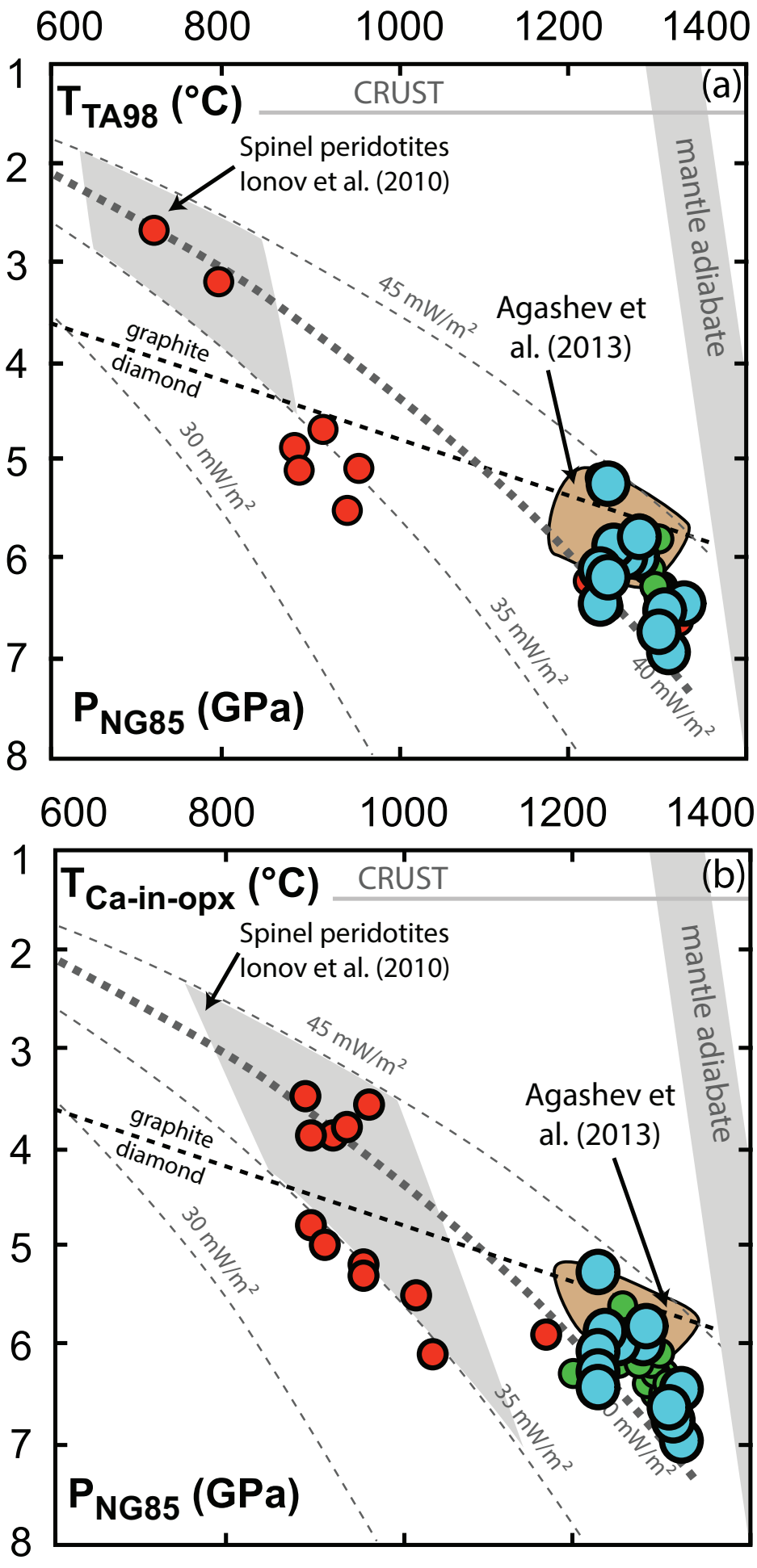
600
800
1000
1200
1400
1
2
3
4
5
6
7
8
T_{TA98} (°C)
CRUST
(a)
Spinel peridotites
Ionov et al. (2010)
mantle adiabate
45 mW/m²
Agashev et
al. (2013)
graphite
diamond
30 mW/m²
35 mW/m²
40 mW/m²
P_{NG85} (GPa)
$T_{Ca\text{-}in\text{-}opx}$ (°C)
CRUST
(b)
Spinel peridotites
Ionov et al. (2010)
mantle adiabate
45 mW/m²
Agashev et
al. (2013)
graphite
diamond
30 mW/m²
35 mW/m²
P_{NG85} (GPa)

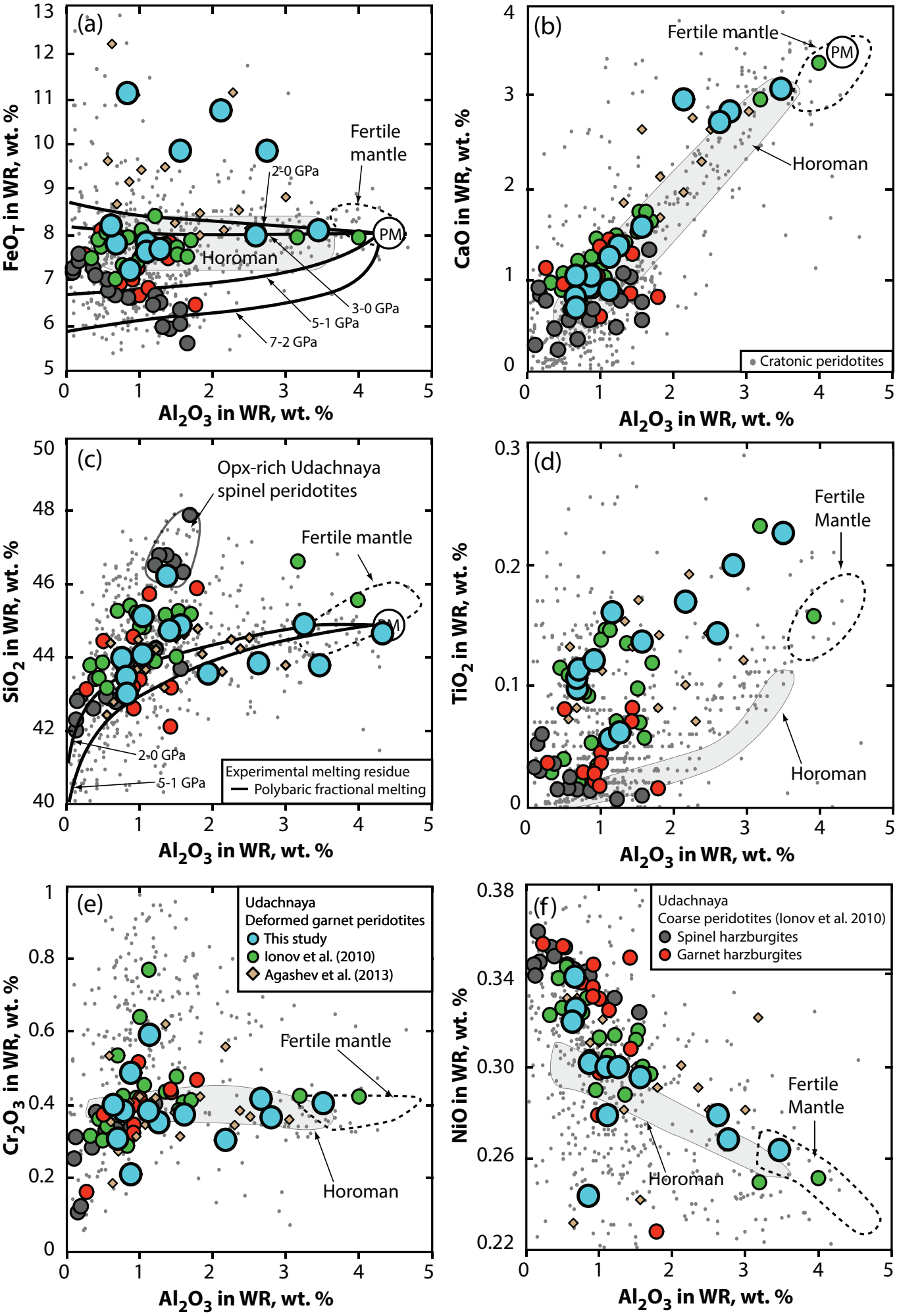
(a)
Fertile mantle
2-0 GPa
PM
Horoman
3-0 GPa
5-1 GPa
7-2 GPa
FeO_T in WR, wt. %
Al_2O_3 in WR, wt. %
(b)
Fertile mantle
PM
Horoman
Cratonic peridotites
CaO in WR, wt. %
Al_2O_3 in WR, wt. %
(c)
Opx-rich Udachnaya spinel peridotites
Fertile mantle
PM
2-0 GPa
5-1 GPa
Experimental melting residue
Polybaric fractional melting
SiO_2 in WR, wt. %
Al_2O_3 in WR, wt. %
(d)
Fertile Mantle
Horoman
TiO_2 in WR, wt. %
Al_2O_3 in WR, wt. %
(e)
Udachnaya
Deformed garnet peridotites
This study
Ionov et al. (2010)
Agashev et al. (2013)
Fertile mantle
Horoman
Cr_2O_3 in WR, wt. %
Al_2O_3 in WR, wt. %
(f)
Udachnaya
Coarse peridotites (Ionov et al. 2010)
Spinel harzburgites
Garnet harzburgites
Fertile Mantle
Horoman
NiO in WR, wt. %
Al_2O_3 in WR, wt. %

Figure 4

Fig. 4

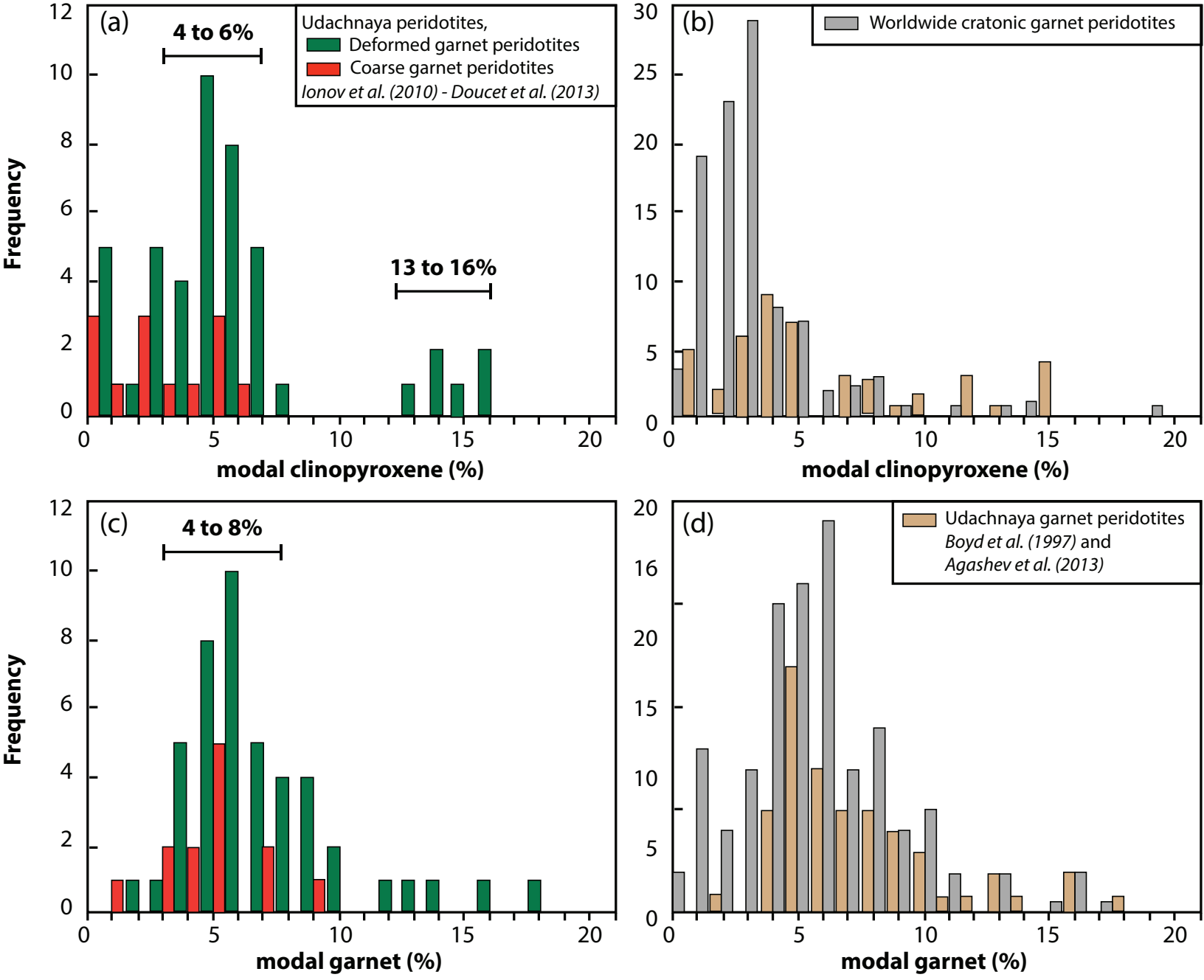

Figure 5

Fig. 5

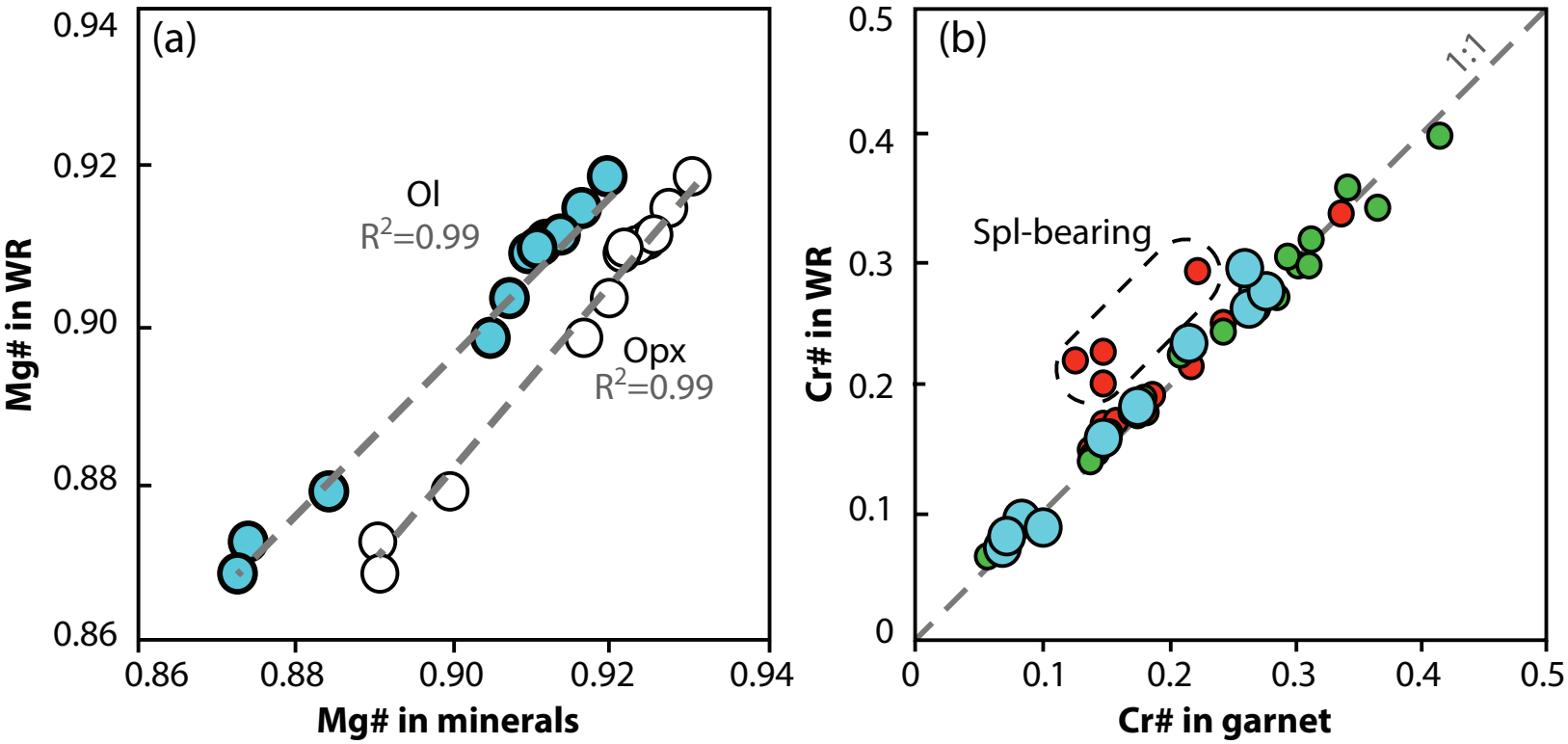

Figure 6

Fig. 6

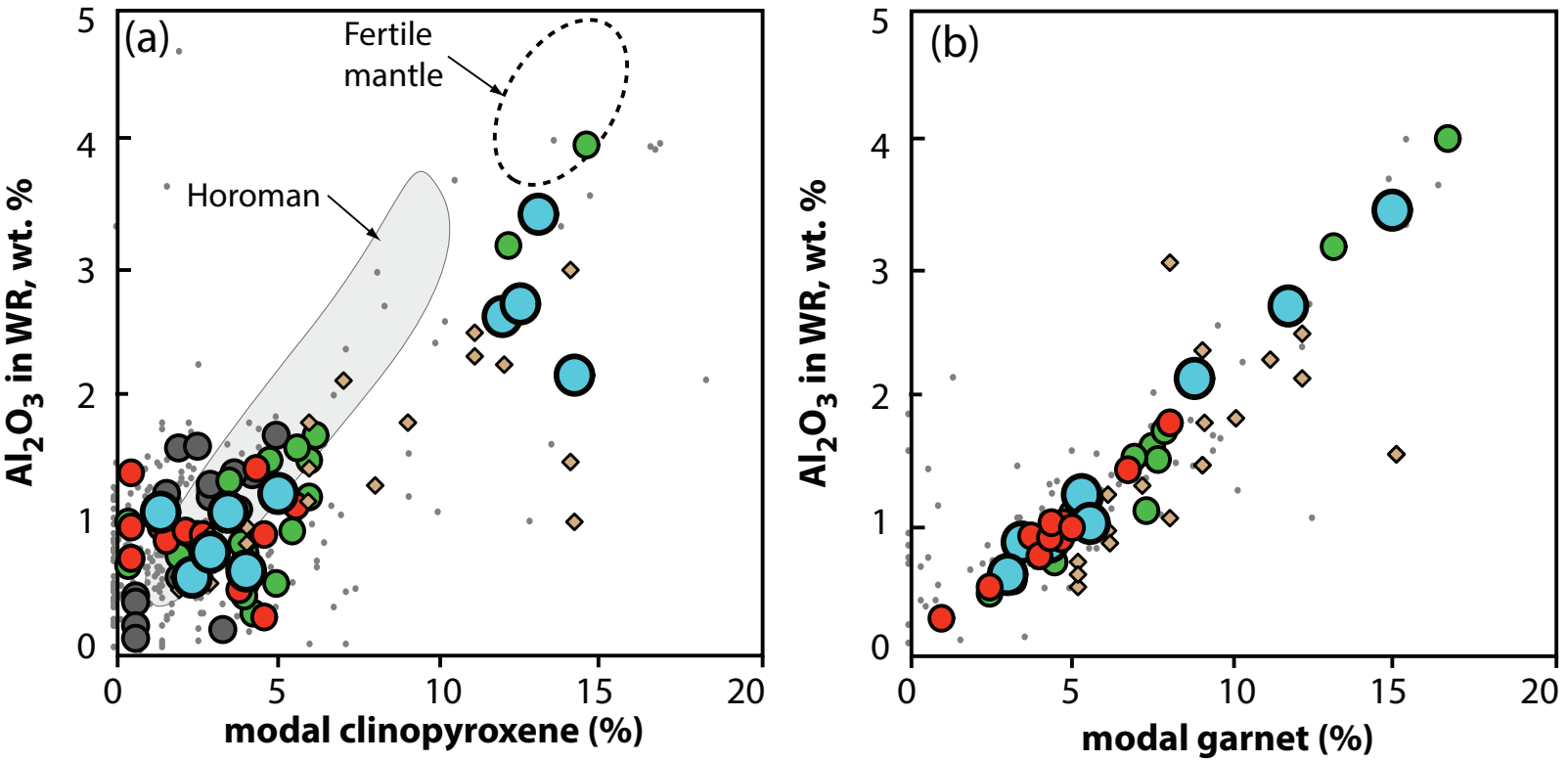

Figure 7

Fig. 7

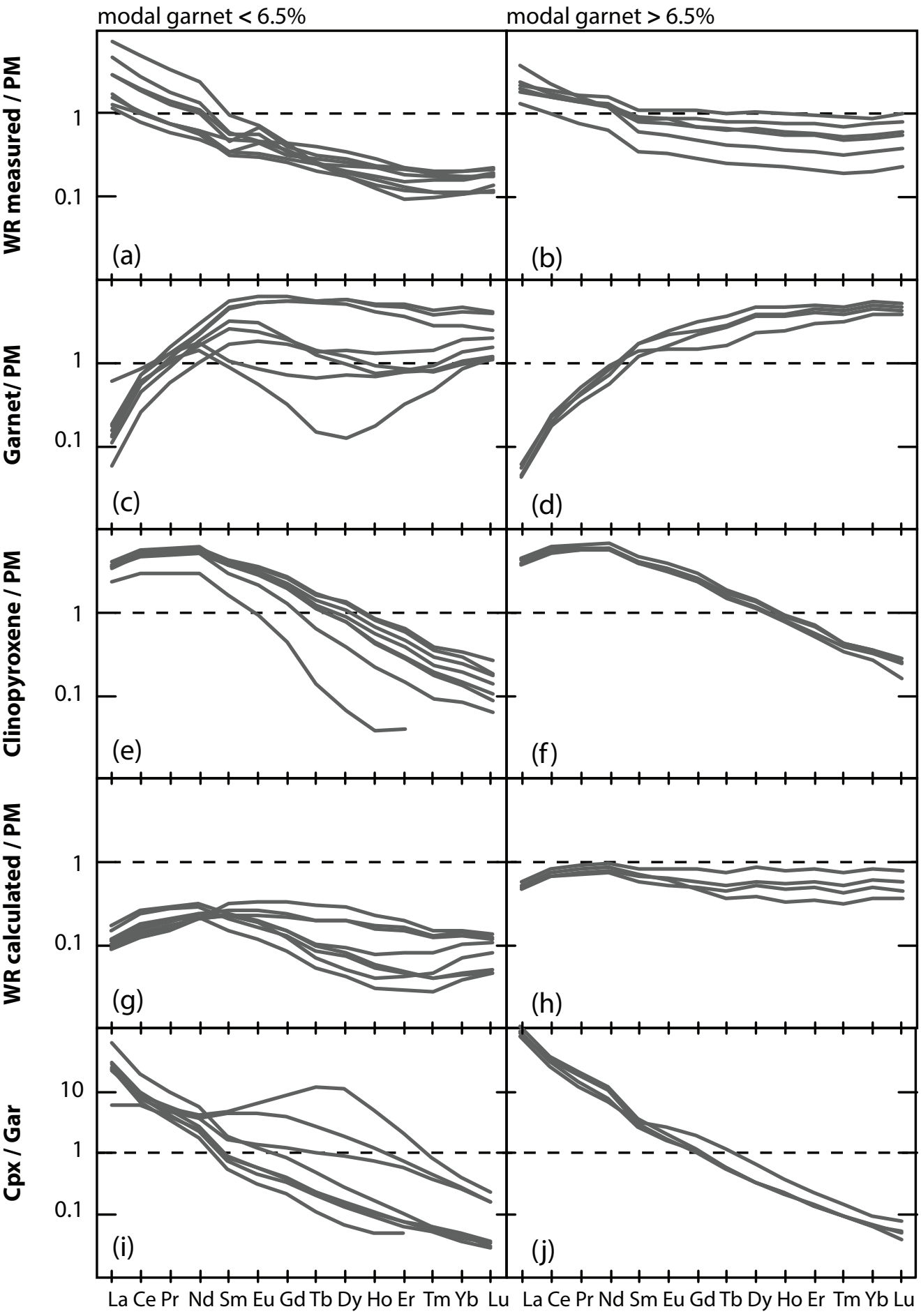

Figure 8

Fig. 8

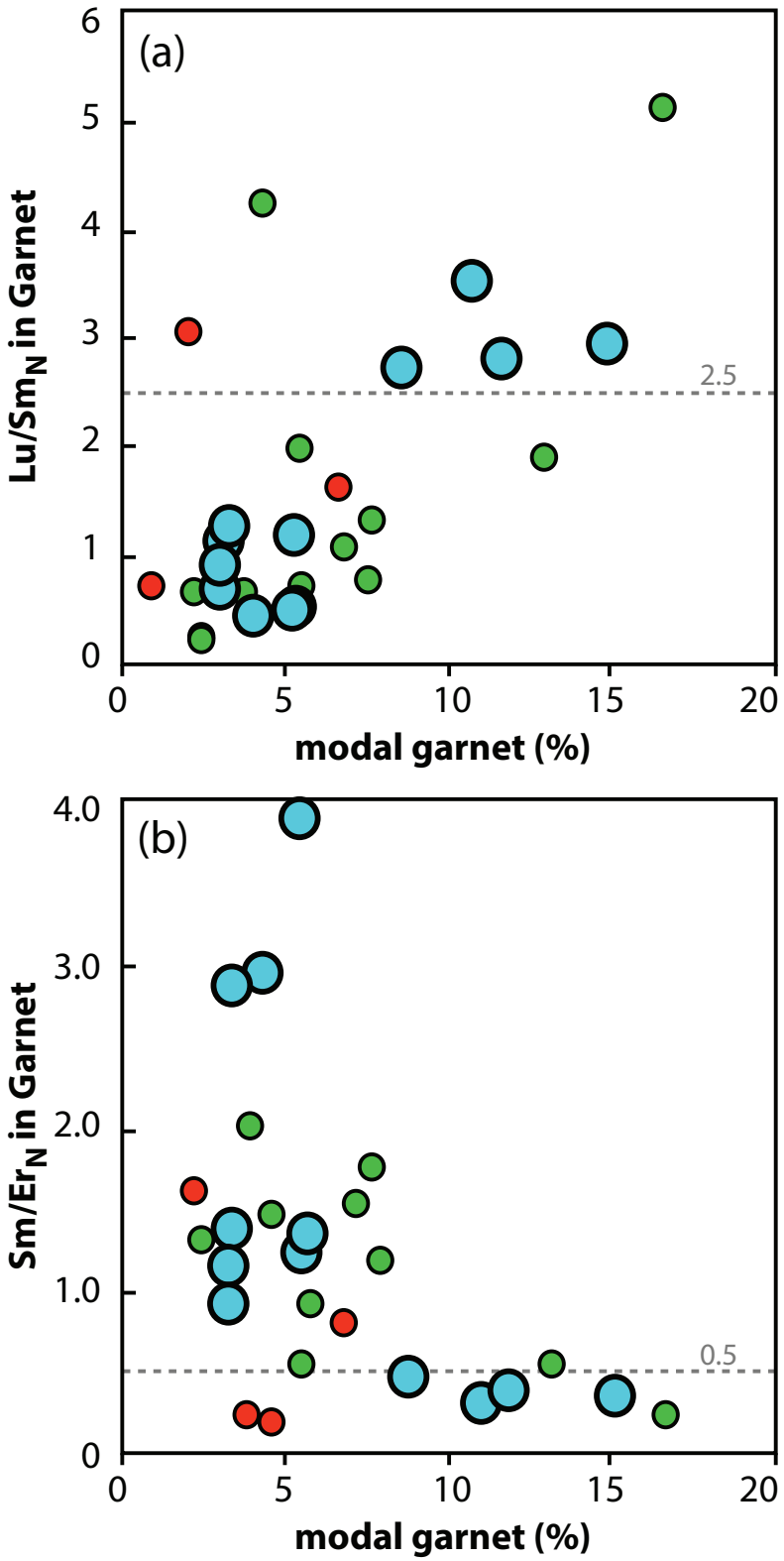

Figure 9

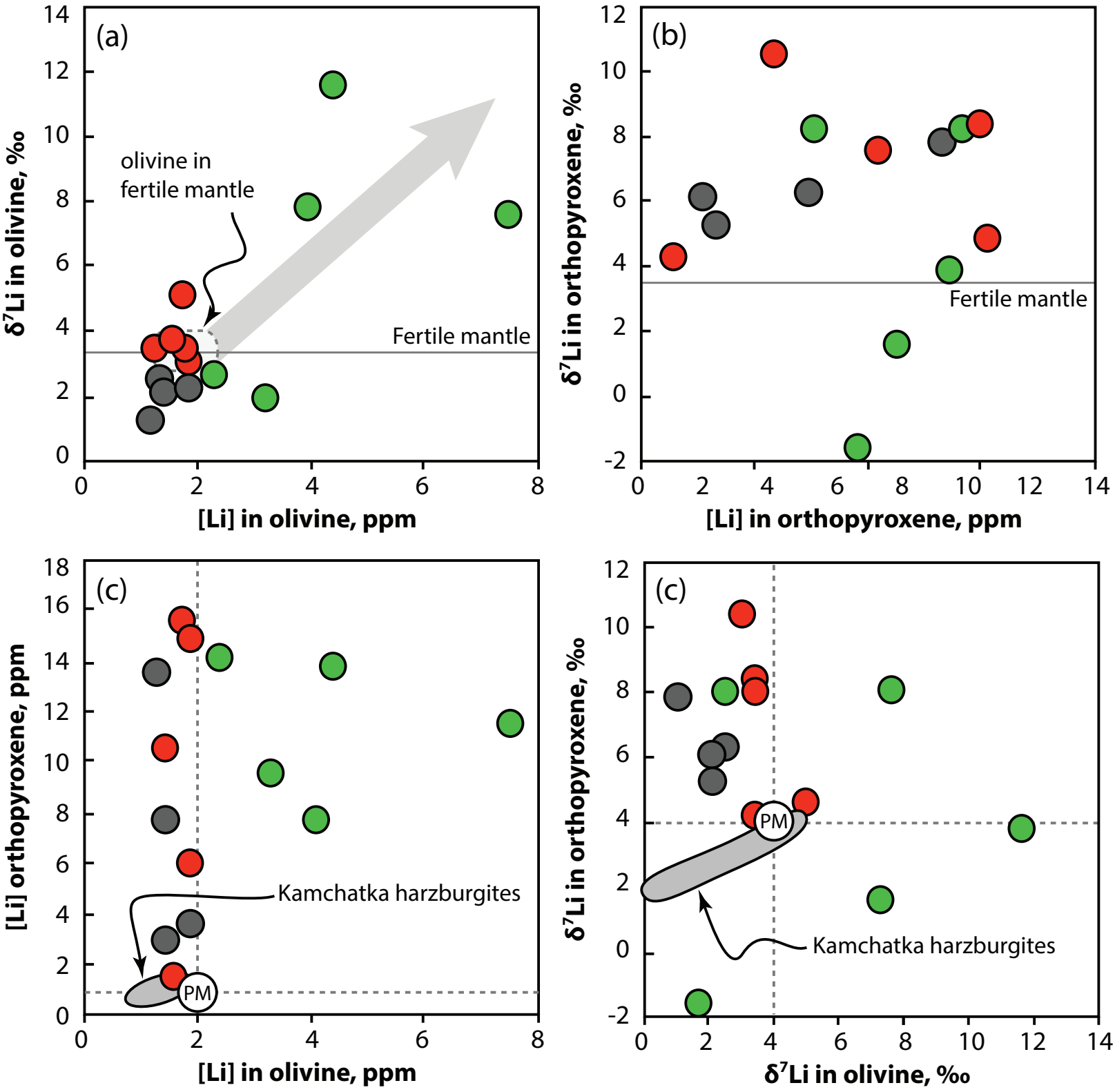
Fig. 9
(a)
olivine in
fertile mantle
Fertile mantle
δ7Li in olivine, ‰
[Li] in olivine, ppm
(b)
Fertile mantle
δ7Li in orthopyroxene, ‰
[Li] in orthopyroxene, ppm
(c)
Kamchatka harzburgites
PM
[Li] orthopyroxene, ppm
[Li] in olivine, ppm
(c)
PM
Kamchatka harzburgites
δ7Li in orthopyroxene, ‰
δ7Li in olivine, ‰

Figure 10

Fig. 10

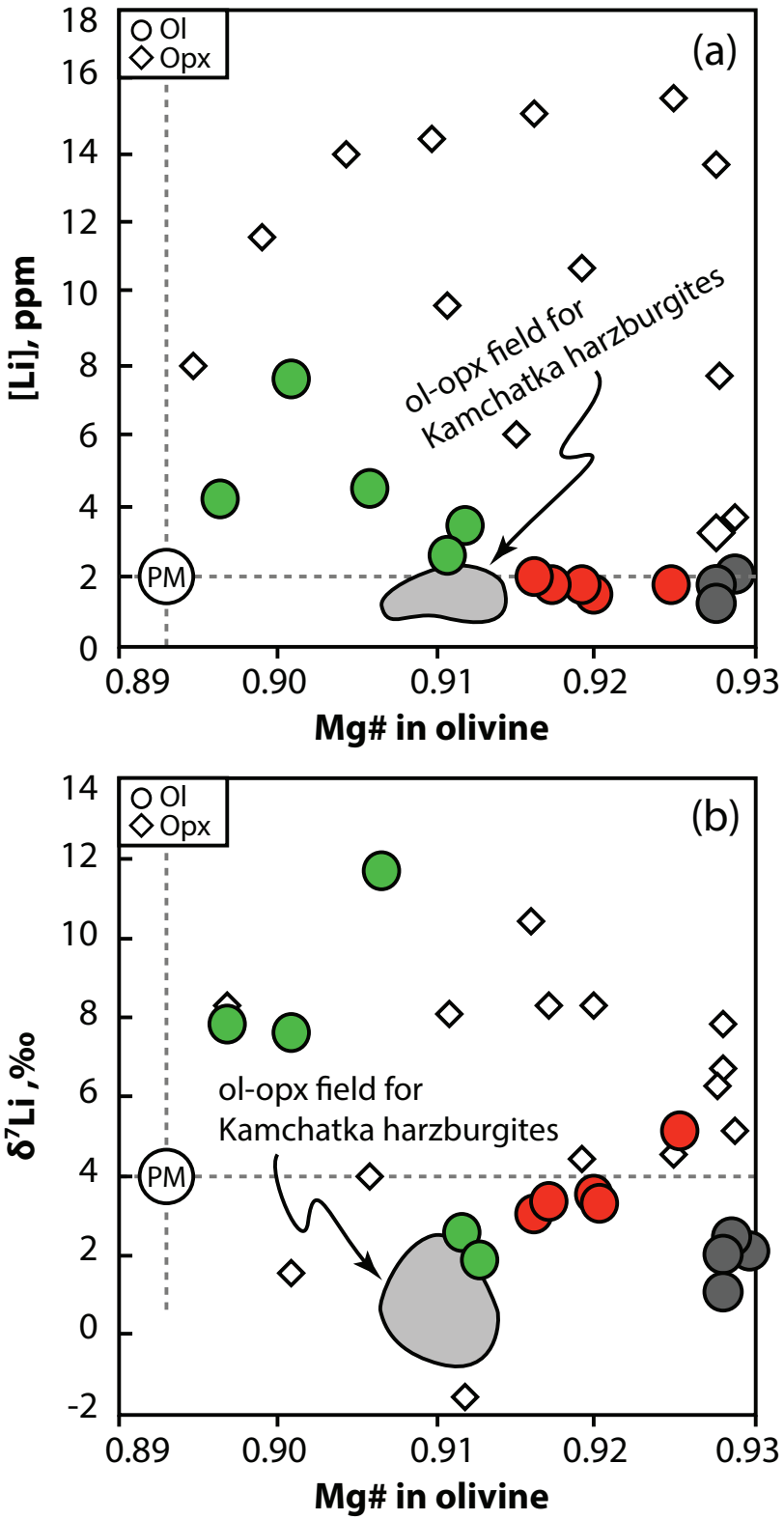

Table 1

Click here to download Table: Table1_SampleList-Deformed.xlsx

Table 1. Summary of petrologic data on new deformed peridotites from Udachnaya in this study.

Sa. No.	Rock	Deformation	P, GPa	T°C	P, GPa	T°C	Modal abundances				WR	Whole-rock composition, wt.%					Ol
	type	degree	P_{NG85}	T_{TA98}	P_{NG85}	$T_{Ca\text{-}in\text{-}opx}$	ol	opx	cpx	gar	g	Al_2O_3	CaO	FeO	Mg#	Ca/Al	Mg#
Uv-405/09	Hz	sheared	61	1238	61	1227	84.1	8.8	3.9	3.2	360	0.68	1.03	7.71	0.915	2.1	0.916
Uv-407/09	Lh	sheared	59	1241	59	1239	66.6	10.8	11.9	10.8	300	2.60	2.73	7.89	0.904	1.4	0.907
Uv-412/09	Lh	sheared	59	1273	59	1274	69.7	7.4	14.3	8.6	330	2.12	2.98	10.64	0.869	1.9	0.873
Uv-424/09	Lh	transitional	60	1268	60	1274	62.2	9.7	13.1	14.9	370	3.45	3.09	8.00	0.899	1.2	0.905
Uv-539/09	Lh	transitional	60	1254	60	1259	68.6	7.1	12.6	11.7	440	2.76	2.86	9.76	0.879	1.4	0.884
Uv-594/09	Hz	sheared	69	1315	70	1324	79.4	15.2	2.3	3.1	350	0.64	0.80	8.14	0.909	1.7	0.910
Uv-533/10	Hz	sheared	65	1332	65	1322	82.4	12.0	2.5	3.1	330	0.67	0.77	8.15	0.910	1.6	0.911
Uv-546/10	Hz	sh-fluidal	64	1237	64	1228	74.1	18.7	3.0	4.1	340	0.86	1.00	7.16	0.919	1.6	0.920
Uv-550/10	Hz-Lh	transitional	62	1240	62	1225	71.6	18.2	4.9	5.3	350	1.23	1.38	7.65	0.911	1.5	0.912
Uv-74/11	Hz	transitional	53	1244	53	1231	75.0	18.7	2.9	3.4	310	0.84	0.93	11.10	0.873	1.5	0.874
Uv-78/11	Hz	transitional	66	1315	66	1311	65.7	27.3	1.6	5.4	380	1.11	0.91	7.68	0.910	1.1	0.911
Uv-110/11	Hz	incipient	67	1307	67	1312	74.0	17.1	3.6	5.3	300	1.12	1.25	7.76	0.912	1.5	0.914
Uv-126/11	Lh	transitional	*n.a.*	*n.a.*	*n.a.*	*n.a.*	*n.a.*	*n.a.*	*5.6*	*6.7*	580	1.57	1.58	9.75	0.887	1.4	*n.a.*

WR, the mass of material from xenolith cores crushed to obtain whole-rock samples.

H, harzburgite; Lh, lherzolite; ol, olivine; opx, orthopyroxene; cpx, clinopyroxene; gar, garnet. Mg#, Mg/(Mg+Fe)at.

Equilibration pressures (P) and temperatures (T) are calculated using two combinations of geothermobarometers; P_{NG85}-T_{TA98} and P_{NG85}-$T_{Ca\text{-}in\text{-}opx}$;

P_{NG85}, opx-gar barometer of Nickel and Green (1985); T_{TA98}, cpx-opx thermometer ofTaylor (1998);

$Tca\text{-}_{in\text{-}opx}$, Ca-in-opx thermometer of Brey & Köhler (1990) corrected as in Nimis and Grütter (2010).

Modal estimates were obtained by least-squares from whole-rock and mineral major oxide compositions

Table 2

Click here to download Table: Table2_Li-samples_Ud.xlsx

Table 2. Petrologic data on xenoliths analyzed for Li-isotopes.

Sample	Rock type	T°C	T°C	P, GPa	Calculated modal abundance (wt.%)					Whole-rock composition, wt.%		
		$T_{Ca\text{-}in\text{-}opx}$	T_{TA98}	P_{NG85}	ol	opx	cpx	gar	sp	Al_2O_3	CaO	Mg#
Spinel peridotites (granular)												
U15	Sp Hz	760	-	≤ *2,5*	63.3	30.7	4.1	0.0	0.4	1.34	1.03	0.930
U24	Sp Hz	885	-	≤ *2,5*	83.3	13.6	2.4	0.0	0.7	0.88	0.63	0.928
U52	Sp Hz	894	-	≤ *2,5*	61.9	34.0	3.7	0.0	0.4	1.40	0.99	0.930
U504	Sp Hz	965	-	≤ *2,5*	84.3	12.7	2.0	0.0	1.0	0.85	0.57	0.929
Granular garnet peridotites												
U260	Gar Hz	871	904	3.9	90.0	4.5	4.5	1.0	0.0	0.27	1.14	0.918
U280	Gar Hz	857	705	2.6	85.1	9.3	1.3	4.3	0.0	1.00	0.60	0.919
U283	Gar-Sp Hz	862	791	3.2	84.4	10.2	1.4	3.7	0.0	0.91	0.59	0.920
U506	Gar Hz	1002	941	5.5	77.2	16.0	2.6	4.2	0.0	0.91	0.94	0.926
U1188	Gar Hz	1340	1331	6.8	69.9	23.1	2.0	5.0	0.0	0.98	1.04	0.917
Deformed garnet peridotites												
U57	Gar Hz-tr	1289	1305	6.6	85.2	8.5	4.0	2.3	0.0	0.44	0.89	0.913
U85	Gar Lh-sh	1198	1240	5.5	57.0	11.9	14.5	16.6	0.0	3.96	3.34	0.897
U148	Gar Lh-sh	1261	1274	6.0	69.7	16.4	6.2	7.7	0.0	1.70	1.65	0.907
U267	Gar Lh-sh	1241	1221	5.4	53.3	21.6	12.1	13.0	0.0	3.17	2.96	0.896
U503	Gar Hz-sh	1288	1323	6.6	75.2	14.0	3.7	7.1	0.0	1.12	1.26	0.912
Kimberlites												
K25-04 (less 10% coarse xenocryst olivine)					/59/					1.89	11.51	0.871
K27-04 (less 18% coarse xenocryst olivine)					/57/					1.53	11.85	0.877

Hz, harzburgite; Lh, lherzolite; ol, olivine; opx, orthopyroxene; cpx, clinopyroxene; gar, garnet; sp, spinel.

Deformation degrees: tr, transitional (low); sh, sheared (high). Mg#, $Mg/(Mg+Fe)_{at}$.

Equilibration temperatures (T) are calculated using two combinations of geothermobarometers; P_{NG85}-T_{TA98} and P_{NG85}-$T_{Ca\text{-}in\text{-}opx}$;

P_{NG85}, opx-gar barometer of Nickel and Green (1985); T_{TA98}, cpx-opx thermometer ofTaylor (1998);

$Tca\text{-}_{in\text{-}opx}$, Ca-in-opx thermometer of Brey & Köhler (1990) corrected as in Nimis and Grütter (2010).

Modal estimates were obtained by least-squares from whole-rock and mineral major oxide compositions

Data for peridotites are from Ionov et al. (2010); data for kimberlites are from Kamenetsky et al. (2012)

Table 3

Click here to download Table: Table3_Li-data_Ud.xlsx

Table 3. Li concentrations and Li and Mg isotope analyses of minerals and bulk rocks for Udachnaya peridotite xenoliths and kimberlites.

Sample	Rock	Ol	Opx	Olivine:			Orthopyroxene		$D^{7}Li$	Measured WR		Calculated WR		P (GPa)	T°C	T°C	Modal abundance		Ol
	type	mg	mg	Li	$d^{7}Li$	$d^{26}Mg$	$d^{7}Li$	Li	ol-opx	Li	$d^{7}Li$	Li	$d^{7}Li$	NG85	Taylor98	BK	ol	opx	Mg#
Spinel peridotites (granular)				ppm	‰	‰	‰	ppm	‰	ppm	‰	ppm	‰				%	%	
U15	Sp Hz	37.5	12.8	1.43	2.04	-0.26	5.98	2.83	-3.9	4.86	7.35	1.8	3.1	*2.5*	-	760	63.3	30.7	0.928
U24	Sp Hz	35.9	13.1	1.41	2.36	-0.20	6.20	7.54	-3.8	6.60	8.64	2.2	2.8	*2.5*	-	885	83.3	13.6	0.928
U52	Sp Hz	34.3	16.6	1.87	2.16		5.15	3.49	-3.0					*2.5*	-	894	61.9	34.0	0.929
U504	Sp Hz	25.6	22.6	1.20	1.17		7.73	13.4	-6.6	6.70	9.11	2.7	2.0	*2.5*	-	965	84.3	12.7	0.928
Averages:				*/1.48/*	*/1.93/*	*-0.23*	*/6.26/*	*/6.82/*		*6.1*	*8.4*	*2.2*	*2.6*						
Granular garnet peridotites																			
U260	Gar Hz	27.0	13.9	1.80	3.35		8.15	15.04	-4.8			2.3	3.4	3.9	904	871	90.0	4.5	0.917
U280	Gar Hz	21.5	11.5	1.62	3.62	-0.26	4.26	1.50	-0.6			1.5	3.5	2.6	705	857	85.1	9.3	0.919
U283	Gar-Sp Hz	57.9	31.2	1.38	3.36		8.19	10.50	-4.8			2.2	3.7	3.2	791	862	84.4	10.2	0.920
U506	Gar Hz	33.4	18.2	1.71	5.04		4.64	15.50	0.4			3.8	4.6	5.5	941	1002	77.2	16.0	0.925
U1188	Gar Hz	39.8	15.3	1.87	3.03		10.3	5.97	-7.3			2.7	4.5	6.8	1331	1340	69.9	23.1	0.916
Averages:				*/1.68/*	*/3.68/*		*/7.11/*	*/9.70/*											
Deformed garnet peridotites																			
U57	Gar Hz-tr	26.0	13.6	2.37	2.52		7.95	14.1	-5.4			3.2	2.8	6.6	1305	1289	85.2	8.5	0.911
U85	Gar Lh-sh	28.2	13.5	7.47	7.45	-0.25	1.51	11.3	5.9			5.6	4.4	5.5	1240	1198	57.0	11.9	0.901
U148	Gar Lh-sh	22.8	27.1	4.39	11.57		3.75	13.7	7.8			5.3	8.7	6.0	1274	1261	69.7	16.4	0.906
U267	Gar Lh-sh	27.1	16.5	4.02	7.75		8.02	7.73	-0.3			3.8	5.9	5.4	1221	1241	53.3	21.6	0.897
U503	Gar Hz-sh	34.2	25.5	3.22	1.80		-1.90	9.45	3.7			3.7	1.1	6.6	1323	1288	75.2	14.0	0.912
Averages:				*4.3*	*6.2*		*3.9*	*11.3*											
Kimberlites																			
K25-04 (less 10% coarse xenocryst Ol)										10.9	7.7								
K27-04 (less 18% coarse xenocryst Ol)										31.8	7.8								

Hz, harzburgite; Lh, lherzolite; WR, whole-rock; ol, olivine; opx, orthopyroxene; cpx, clinopyroxene; gar, garnet, spl, spinel.

The mass (mg) of pure olivine and opx separates used for the analyses is provided. See Table 1 for descriptions for descriptions of P-T methods.

Whole-rock values of [Li] and $d^{7}Li$ were calculated from measured [Li] and $d^{7}Li$ values and modal abundances of olivine and opx.

The long-term reproducibility, as determined by repeated analyses of international reference materials over 8 years, is ±0.3‰ (2s) for $d^{7}Li$ and 0.06‰ for $\delta^{26}Mg$

Background dataset for online publication only

Click here to download Background dataset for online publication only: ES1_NewSheared.xlsx

Background dataset for online publication only

Click here to download Background dataset for online publication only: ES2_SamplesForLi-isot.xlsx